

Dear Editor,

Thank you for handling our manuscript. We are grateful to the reviewers for their comments and suggestions. Originally, we focused our analysis and discussion mainly on chemical processes. In response to the reviewers' comments, we extended our analysis to dynamical processes using backward trajectories, radiosonde and ground-based remote sensing data. We revised our manuscript and supplement by including the results and discussion of the additional analysis. We made a structural change by dividing the contents in section 3 into several subsections. We also made some other changes necessary and corrected error we identified. Here are our responses (in blue) to reviewers' comments and changes (highlighted in yellow) in manuscript and supplement.

Xiaobin Xu on behalf of all co-authors

Response to Reviewer #1:

This manuscript comments on the study of Chen et al. (2022), proposing that the nocturnal O₃ enhancement (NOE) on 31 July 2021 over the North China Plain is caused by the stratosphere O₃ intrusion after the passage of Typhoon In-fa. The authors argue that the NOE is instead due to the photochemically produced O₃, which can be brought downward from the residual layer at night. Overall, the manuscript is well-written, and the method is reasonable. I have a few points that I think could be addressed to strengthen the manuscript and some minor comments.

Response: We thank the reviewer for the positive comments and suggestions. Here are our point-to-point responses to the comments.

General Comments:

1. Although I tend to believe that STT usually has little effect on ground O₃ at low altitudes, the reasoning in the manuscript needs to be further elaborated. Could you explain more on why higher nighttime Ox than daytime O₃ is an indicator of downward mixing from the residual layer and vice versa? Also, both O₃ and PAN can be transported over long distances, and I am not sure why the in-phase changes of O₃ and PAN could exclude the possibility of STT. Lastly, the authors mention that HOLWCO could also occur in photochemically aged air, not necessarily from STT, but the photochemical age analysis in the manuscript shows fresh air with ages less than 10 hrs. Does that mean HOLWCO can occur in fresh air as well?

- Could you explain more on why higher nighttime Ox than daytime O₃ is an indicator of downward mixing from the residual layer and vice versa?

Response: Our intention is to check whether or not surface O₃ observed during the

NOE contained significant contribution of O_3 from the stratosphere. For this purpose, a comparison of O_3 levels in the vertical direction is helpful. However, O_3 is very reactive and can be significantly removed by titration reactions in the boundary layer, with $O_3 + NO = NO_2 + O_2$ being the most important one. Therefore, O_x (O_3+NO_2) is a more conserved quantity than O_3 and hence a better metric for comparison (Kley et al., 1994; Kleinmann et al., 2002; Caputi et al., 2019; He et al., 2022). During daytime, NO_2 formed in the titration reaction is rapidly photolyzed to regenerate O_3 so that the net chemical loss of O_3 is relatively small. At night, however, the reaction between O_3 and NO leads to lower levels of O_3 in the nocturnal boundary layer (NBL) and in the residual layer (RL). Because the emission of NO takes place mainly in the NBL, much more O_3 is removed by the titration reaction in the NBL than in the RL (Wang et al., 2018; Caputi et al., 2019; He et al., 2022). In addition, O_3 in the NBL is subjected to dry deposition. Therefore, the O_3 level before sunset largely remains in the RL (Caputi et al., 2019; He et al., 2022) and is usually much higher in the RL than in the NBL under normal conditions.

Following the method of He et al. (2022), we make comparison of afternoon O_3 averages on 31 July with the respective O_x averages in the NBL during the NOE between 31 July and 1 August, 2021. To facilitate the comparison, we treat the average surface O_3 during 14:00-17:00 LT of 31 July as afternoon average of O_3 in the convective boundary layer, denoted as $[O_3]_{aft}$. Let us now focus on three nighttime atmospheric conditions, (I) undisturbed, (II) disturbed with NOE but no STT impact, and (III) disturbed with NOE and significant STT impact.

Under undisturbed condition (I), the nighttime average O_3 concentration in the RL ($[O_3]_{RL}$) should be close to (or only slightly lower than) $[O_3]_{aft}$ (Caputi et al., 2019; He et al., 2022), while the average O_3 concentration in the NBL ($[O_3]_{NBL}$) should be much lower than $[O_3]_{aft}$ due to the impacts of NO titration ($\Delta[O_3]_{titr}$) and dry deposition ($\Delta[O_3]_{dep}$), and the average O_x concentration in the NBL ($[O_x]_{NBL}$) should also be lower than $[O_3]_{aft}$ due to dry deposition. The following relationships should be tenable:

$$[O_3]_{RL} \leq [O_3]_{aft} \quad (1)$$

$$[O_3]_{NBL} = [O_3]_{aft} - \Delta[O_3]_{titr} - \Delta[O_3]_{dep} \quad (2)$$

$$[O_x]_{NBL} = [O_3]_{aft} - \Delta[O_3]_{dep} \quad (3)$$

Under disturbed condition with NOE but no STT impact (II), a downward transport of O_3 from the RL to NBL should be considered. Assuming that the downward transport causes a reduction of $[O_3]_{RL}$ by $\Delta[O_3]_{D1}$ and an increase of $[O_3]_{NBL}$ by $\Delta[O_3]_{D2}$, then

$$[O_3]_{RL} \leq [O_3]_{aft} - \Delta[O_3]_{D1} \quad (4)$$

$$[\text{O}_3]_{\text{NBL}} = [\text{O}_3]_{\text{aft}} - \Delta[\text{O}_3]_{\text{titr}} - \Delta[\text{O}_3]_{\text{dep}} + \Delta[\text{O}_3]_{\text{D2}} \quad (5)$$

$$[\text{O}_x]_{\text{NBL}} = [\text{O}_3]_{\text{aft}} - \Delta[\text{O}_3]_{\text{dep}} + \Delta[\text{O}_3]_{\text{D2}} \quad (6)$$

Under disturbed condition with NOE and STT impact (III), net contributions of O_3 from the STT should be considered to the RL and the NBL. Assuming that the STT contribution increases $[\text{O}_3]_{\text{RL}}$ and $[\text{O}_3]_{\text{NBL}}$ by $\Delta[\text{O}_3]_{\text{STT1}}$ and $\Delta[\text{O}_3]_{\text{STT2}}$, respectively, then

$$[\text{O}_3]_{\text{RL}} \leq [\text{O}_3]_{\text{aft}} + \Delta[\text{O}_3]_{\text{STT1}} \quad (7)$$

$$[\text{O}_3]_{\text{NBL}} = [\text{O}_3]_{\text{aft}} - \Delta[\text{O}_3]_{\text{titr}} - \Delta[\text{O}_3]_{\text{dep}} + \Delta[\text{O}_3]_{\text{STT2}} \quad (8)$$

$$[\text{O}_x]_{\text{NBL}} = [\text{O}_3]_{\text{aft}} - \Delta[\text{O}_3]_{\text{dep}} + \Delta[\text{O}_3]_{\text{STT2}} \quad (9)$$

Equation (3) indicates that $[\text{O}_x]_{\text{NBL}}$ should be significantly lower than $[\text{O}_3]_{\text{aft}}$ under undisturbed conditions. Although equation (6) shows that $[\text{O}_x]_{\text{NBL}}$ could be higher than $[\text{O}_3]_{\text{aft}}$ (i.e., if $\Delta[\text{O}_3]_{\text{dep}} < \Delta[\text{O}_3]_{\text{D2}}$), it cannot really occur because $[\text{O}_3]_{\text{RL}} < [\text{O}_3]_{\text{aft}}$ (see equation (4)) and O_3 cannot be transported from a lower concentration position to the higher one. Therefore, $[\text{O}_x]_{\text{NBL}}$ should not be significantly higher than $[\text{O}_3]_{\text{aft}}$ under disturbed conditions with NOE but no STT impact. Dry deposition is only a small sink for nighttime surface O_3 in northern China (Tang et al., 2017), while a STT impact could substantially enhanced the level of surface O_3 if it reaches the surface layer. Hence, it is very likely according to equation (9) that $[\text{O}_x]_{\text{NBL}}$ is significantly higher than $[\text{O}_3]_{\text{aft}}$ under disturbed condition with a STT impact. In summary, $[\text{O}_x]_{\text{NBL}}$ should be significantly higher than $[\text{O}_3]_{\text{aft}}$ if the NBL is really impacted by stratospheric O_3 , otherwise the STT impact is negligible even though a NOE event is observed.

As shown in Table 1 in our manuscript, in all cities but Weihai (WH), mean O_x during the maximum NOE period was either much lower than or nearly equal to mean O_3 during the afternoon period. This indicates that O_3 in the NBL in those cities was probably not impacted by stratospheric O_3 . Mean O_x in WH during the NOE was much higher than mean O_3 in the erstwhile afternoon. However, this could not be attributed to stratospheric impact. Chen et al. (2022) mentioned “the surface ozone enhancement at midnight was not coincident with CO reduction, suggesting that the stratospheric air mass might not have reached the surface.” (at the end of the second paragraph in section 4.2). The higher $[\text{O}_x]_{\text{NBL}}$ in WH may also be interpreted by the above equation (6), i.e., if $\Delta[\text{O}_3]_{\text{D2}}$ was much greater than $\Delta[\text{O}_3]_{\text{dep}}$. A great $\Delta[\text{O}_3]_{\text{D2}}$ would require a high $[\text{O}_3]_{\text{aft}}$, either from local photochemical production or from transport. Actually, photochemically produced O_3 (PPO) had not been well established in WH during the daytime on 31 July, as can be seen in our Figure 1f. Therefore, regional-scale transport of PPO is suspected. In section 3 of our manuscript, we provided an interpretation in the viewpoint of diurnal alternations of land-sea breezes. Our view is supported by the backward trajectories shown in Figure 1R(right), which indicate that air parcels influenced the

NBL in WH were mostly from the Yellow Sea area. The prevailing wind direction at 850 hPa over the Yellow Sea and the neighboring land was SW, as shown in Figure 5 (a) in Chen et al. (2022). Such wind condition could facilitate the transport of PPO from the continent to the sea area. Because of the lower emissions of NO_x over the sea, PPO can be well sustained at night and transported to continental locations like WH through sea breezes.

In Figure R1, we also show 24-h backward trajectories arriving at 100 m above ground over ZB and BZ. All the trajectories do not indicate any transport of air parcels from altitudes over daytime boundary layer. Figure R2 shows a matrix of backward trajectories for air parcels arriving at 100 m above ground over the domain 36°38' N and 115°122' E at 19:00 UTC, 31 July 2021. Only 3 of the 24 trajectories were ever travelled over daytime boundary layer and the 3 trajectories ended at locations over the Bohai Gulf.

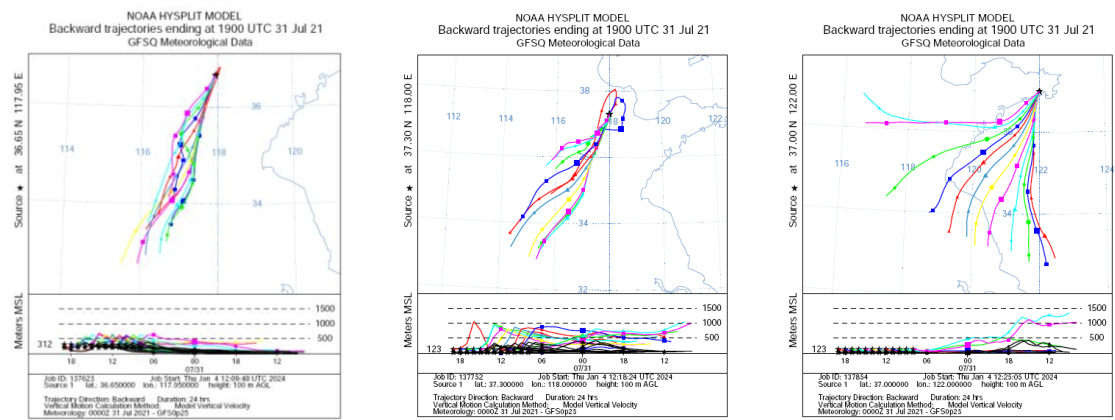


Figure R1. Backward trajectories for air parcels arriving at 100 m above ground over Zibo (ZB, left), Binzhou (BZ, middle) and Weihai (WH, right) every hour between 19:00 and 08:00 UTC, 31 July 2021. The trajectories were computed online using the HYSPLIT model (<https://www.ready.noaa.gov/HYSPLIT.php>; Stein et al. 2015; Rolph et al., 2017) and the Global Forecast System (GFS) reanalysis data (0.25 ° resolution, https://www.emc.ncep.noaa.gov/ems/pages/numerical_forecast_systems/gfs.php). The total run time for the trajectories was 24 hours.

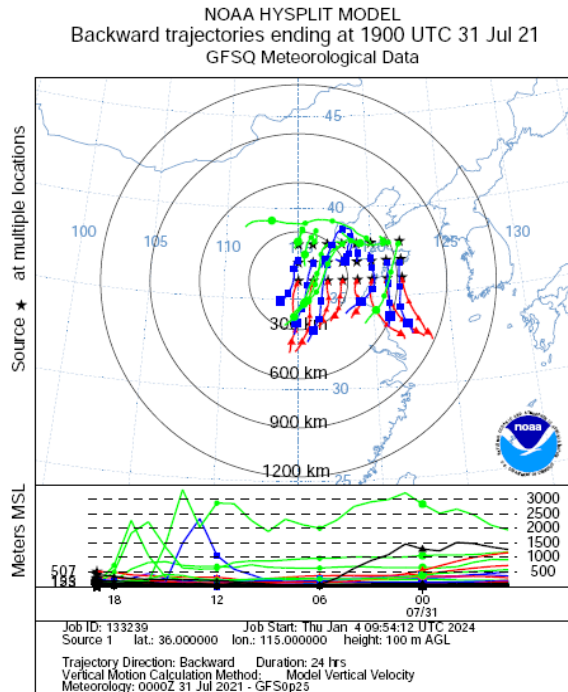


Figure R2. Matrix of backward trajectories for air parcels arriving at 100 m above ground over the domain 36°38' N and 115°122' E at 19:00 UTC, 31 July 2021. The trajectories were computed online using the HYSPLIT model (<https://www.ready.noaa.gov/HYSPLIT.php>; Stein et al. 2015; Ralph et al., 2017) and the Global Forecast System (GFS) reanalysis data (0.25° resolution, https://www.emc.ncep.noaa.gov/emc/pages/numerical_forecast_systems/gfs.php). The total run time for the trajectories was 24 hours.

In addition to the backward trajectories, some ground-based remote sensing data also support our view. Figure R3 presents time-altitude cross sections of O_3 , relative humidity, virtual temperature and wind speed observed at the ZB supersite between 18:00 LT, 31 July and 06:00 LT, 1 August 2021. As can be seen in the figure, relatively higher O_3 mixing ratios occurred only below about 0.5 km. From the evening to midnight, very strong wind prevailed below 1 km, after which humidity was largely enhanced, it rained and the NOE event occurred. The top of the higher O_3 layer was partly uplifted during the NOE period. According to the backward trajectories shown in Figure R2 (left), the air parcels were from the southwest sector and travelled mostly below 0.5 km above sea level. There was no indication of air from the free troposphere. And it is very likely that the NOE was due to horizontal transport of daytime PPO from the southwest sector.

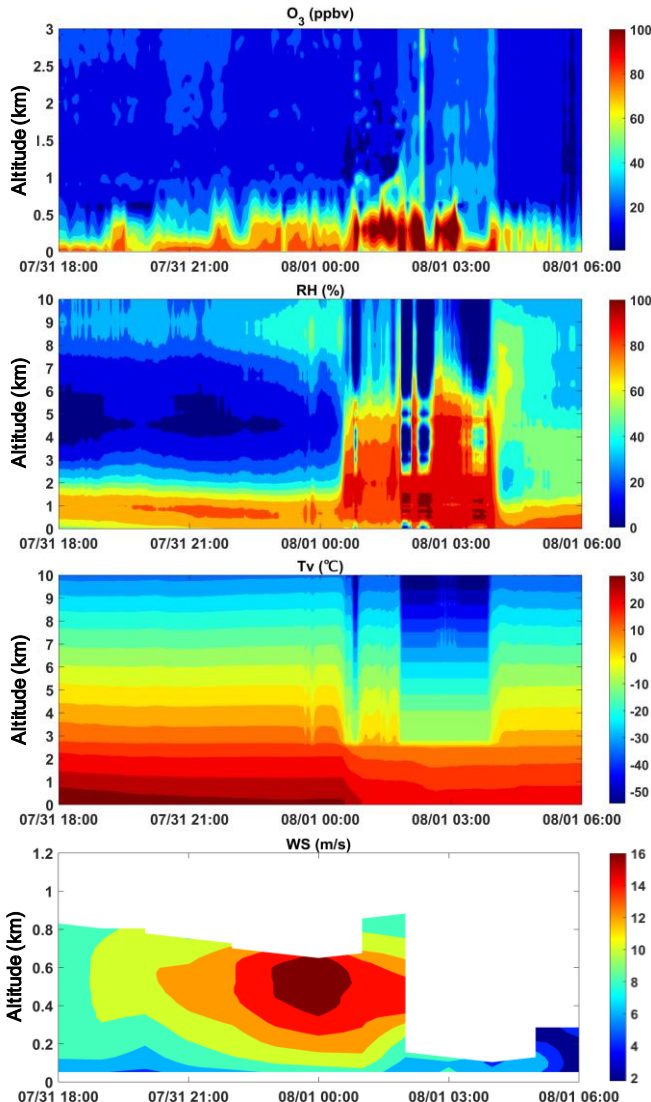


Figure R3. Time-altitude cross sections of O_3 , relative humidity (RH), virtual temperature (Tv) and wind speed (WS) observed at the ZB supersite between 18:00 LT, 31 July and 06:00 LT, 1 August 2021.

In conclusion, our comparisons of nighttime O_x with daytime O_3 in the NCP cities and analysis of backward trajectories and remote sensing data suggest that the NOE events observed at the NCP cities were most likely from the transport of O_3 in the RL or (in the case of WH) in the marine boundary layer, and unlikely from the transport of stratospheric O_3 .

We included the discussion about the comparison between afternoon O_3 and O_x in the NBL in the revised supplement as Text S1 (lines 77-122), changed the original Text S1 to Text S2 and renumbered the equations and figures.

“Text S1 Identifying potential origin of the NOE by comparing afternoon O_3 with O_x in the NBL during the NOE

Our intention is to check whether or not surface O_3 observed during the NOE contained significant contribution of O_3 from the stratosphere. For this purpose, a comparison of O_3 levels in the

vertical direction is helpful.In summary, $[O_x]_{NBL}$ should be significantly higher than $[O_3]_{aft}$ if the NBL is really impacted by stratospheric O_3 , otherwise the STT impact is negligible even though a NOE event is observed.”

In section 3.2 in the revised manuscript, we cited Text S1 and changed text as follows:

“Following the method of He et al. (2022), we make comparison of O_3 averages during 14:00-17:00 LT on 31 July in the above cities with the respective O_x (O_3+NO_2) averages during the periods of the maximum NOE between 31 July and 1 August (Table 1). Such comparison facilitates the judgment whether or not the NOE was caused by downward mixing of air in the residual layer (RL) into the nocturnal boundary layer (NBL) because afternoon averages of O_3 in the convective boundary layer are well preserved at night in the RL and O_x is a more conserved quantity than O_3 in the NBL. Details about the reasonability of this method are given in Text S1. It can be seen in Table 1 that, except for WH, the nighttime O_x averages approach to or obviously lower than the respective daytime O_3 averages. In the mega-cities QD and JN, the average levels of O_x during the maximum NOE were nearly the same as those of daytime O_3 , while the nighttime O_x in the other cities (excluding WH) was at least a few ppbv lower than daytime O_3 . According to the discussions in Text S1, for all cities excluding WH, data in Table 1 do not suggest any significant STT impact on the NOE events.”

We included Figures R1 and R2 in the revised supplement as Figures S3 and S4. We cited Figures S3 and S4 in section 3.3 in the revised manuscript and changed the text about influences of land-sea breezes on WH:

“The case of WH deserves more detailed analysis. WH is a relatively smaller city in the tip of the Shandong Peninsula. The higher O_x concentration for WH in Table 1 was probably related to the regional transport of air pollution and the influence of the diurnal alternations of land-sea breezes. Actually, the afternoon PPO in WH had not been well established as shown in Figure 1f. During the daytime (particularly afternoon), when sea breeze dominates, PPO is significantly diluted by cleaner air from the marine boundary layer. The daily maximum of O_3 in WH is generally observed between 11:00 LT and 13:00 LT, rather than between 14:00 LT and 17:00 LT. If the O_3 average for WH in Table 1 were replaced with that from 11:00 LT to 13:00 LT on 1 August (80 ± 2.0 ppbv), then the difference between O_x and O_3 would be reduced to about 21 ppbv. At night, when the land breeze dominates, the near surface level of WH is usually controlled by divergence, which induces downdraft from the residual layer, transports daytime PPO residing in the residual layer to the surface, and resulted in the NOE. This might have been the main reason of highly frequent NOE emerging in WH. ”

We added two paragraphs in section 3.3 to extend our discussion on atmospheric transport:

“Chen et al. (2022) investigated the atmospheric transport process of the NOE by using high-resolution Weather Research and Forecasting (WRF) simulation and FLEXible PARTicle (FLEXPART) particle dispersion modelling. They presented the two scenarios for BZ and QD and found very different results for the two cities. To support above view, we calculated backward

trajectories of air parcels arriving at 100 m above ground level over WH every hour between 19:00 and 08:00 UTC, 31 July 2021 using HYSPLIT model (<https://www.ready.noaa.gov/HYSPLIT.php>) and the Global Forecast System (GFS) reanalysis data (0.25 °resolution, https://www.emc.ncep.noaa.gov/emc/pages/numerical_forecast_systems/gfs.php). Our intention is not to resolve the dynamical evolution of the MCSs but to analyze atmospheric transport at a relatively larger scale. Figure S3 shows the calculated backward trajectories for WH, together with those for ZB and BZ in the same time window. The trajectories in Figure S3(right) indicate that air parcels influencing the NBL in WH were mostly from the marine boundary layer over the Yellow Sea area. The prevailing wind direction at 850 hPa over the Yellow Sea and the neighbouring land was SW, as shown in Figure 5a in Chen et al. (2022). Such wind condition could facilitate the transport of PPO from the continent to the sea area. Because of the lower emissions of NO_x over the sea, PPO can be well sustained at night and transported to continental locations like WH through sea breezes.

The 24-h backward trajectories for ZB (Figure S3(left)) and BZ (Figure S3(middle)) provide additional clues denying STT impacts on nighttime O₃ in these cities. All the trajectories do not indicate any transport of air parcels from altitudes over daytime boundary layer. To gain a more complete insight into the air movements during and before the NOE events, we show in Figure S4 a matrix of backward trajectories for air parcels arriving at 100 m above ground level over the domain 36 °38 N and 115 °122 E at 19:00 UTC (03:00 LT), 31 July 2021. The trajectory heights and locations shown in Figure S4 indicate that only 3 of the 24 trajectories travelled over daytime boundary layer and the 3 trajectories ended at locations over the Bohai Gulf. Therefore, our systematic trajectory analysis does not suggest that the NOE events in the NCP cities were related with downward transport of airmasses from the free troposphere.”

We included Figure R3 in the revised supplement as Figure S8 and added profiles of wind vector as Figure S9. We made section 3.6 in the revised manuscript to cite these figures and discuss the results as follows:

“In addition to the backward trajectories, some ground-based remote sensing data from ZB also support our view. Figure S8 presents time-altitude cross sections of O₃, relative humidity (RH), virtual temperature (Tv) and wind speed (WS) observed at the ZB supersite between 18:00 LT, 31 July and 06:00 LT, 1 August 2021. As can be seen in the figure, relatively higher O₃ mixing ratios occurred only below about 0.5 km. From the evening to midnight, very strong wind prevailed below 1 km, after which humidity was largely enhanced, it rained and the NOE event occurred. The wind directions below 1 km were southerly before 01:00 LT and turned to northerly by 02:00 LT (Figure S9). The top of the higher O₃ layer was partly uplifted during the NOE period. According to the backward trajectories shown in Figure S3(left), the air parcels were from the southwest sector and travelled mostly below 0.5 km above sea level. Both the remote sensing data and the trajectory analysis provide no evidence of air from the free troposphere. Therefore, it is very likely that the NOE observed from the ground to about 0.5 km was due to advection transport of daytime PPO from the southwest sector rather than SST impacts.”

- Also, both O₃ and PAN can be transported over long distances, and I am not sure why

the in-phase changes of O₃ and PAN could exclude the possibility of STT.

Response: Indeed, both O₃ and PAN can be transported over long distances at higher altitudes, where their chemical removal is limited. However, PAN is primarily produced where VOCs and NO_x are largely emitted, such as in industrial and populated areas or in biomass burning plumes (Xu et al., 2018). Higher temperatures and intense radiation are favorable meteorological conditions for the formation of PAN. These chemical and meteorological conditions facilitate the production of O₃ as well. For this reason, O₃ and PAN in the boundary layer are usually well correlated, particularly in warm seasons. The in-phase changes of O₃ and PAN reflect the dominant influences of chemical and physical processes within the boundary layer but do not exclude the possibility of STT. What really do not support the possibility of STT is the relatively higher value of PAN observed during the NOE at the ZB supersite. The average PAN (0.44±0.02 ppbv) was higher than the lowest nighttime PAN levels on most days before and after the NOE event. This evidence disproves the possibility of significant STT impact.

Lacking of parallel measurements of PAN at high altitudes over the NCP hinders us from making a vertical comparison of PAN levels. However, some PAN values from earlier high altitude observations can be referenced. The PAN values in the UTLS over the NCP in August 2003 ranged from about 0.17 ppb (at 185 hPa) to 0.35 ppb (at 278 hPa), as retrieved from the satellite observations (Moore and Remedios, 2010). Ten-years of satellite observations showed that average PAN in the UTLS over the anticyclone region (60–120°E, 10–40°N) reached its maximum in summer and varied in the range of 0.06-0.3 ppb (Fadnavis et al., 2014). Aircraft measurements of PAN in July 2008 over Longyearbyen, Spitsbergen (78°130'N, 15°330'E) and Oberpfaffenhofen, Germany (48°40'N, 11°160'E) showed PAN levels in the range of 0.05-0.3 ppb in the free troposphere and lower stratosphere (Roiger et al., 2011). Airborne measurements over North America showed summer PAN in the free troposphere and lowermost stratosphere were usually lower than 0.5 ppb unless biomass burning air masses were sampled (Singh et al., 2007). Observations at high mountain sites also indicated quite low PAN levels in the free troposphere. For example, multiyear observations at the high alpine site Jungfraujoch (46.55°N, 7.98°E, 3580 m.a.s.l) found average summer PAN levels of lower than 0.2 ppb in free tropospheric air masses (Pandey Deolal et al., 2013) and those at Summit station, Greenland (72.34°N, 38.29°W, 3212 m.a.s.l.) showed average summer PAN levels of lower than 0.1 ppb (Kramer et al., 2015). In summary, the mixing ratios of PAN in the free troposphere and lower stratosphere of the Northern Hemisphere are normally much lower than 0.5 ppb and mostly lower than 0.3 ppb.

PAN is thermally unstable and decomposes rapidly in warm urban air. According to Cox and Roffey (1977), the lifetime of PAN was only 2.7 hours at 25 °C. In our case,

the nighttime temperature at the ZB supersite varied from 33.1 °C at 18:00 LT on 31 July to 20.4 °C at 06:00 LT on 1 August, 2021, with an average of 26.0 °C. Under such warm condition, even shorter lifetimes of PAN are expected. The thermal decomposition lifetimes were in the range of 0.2-1.3 hours based on the hourly observations. If the surface layer had been significantly impacted by air masses from the free troposphere and lower stratosphere, we would have seen much lower levels of PAN during the NOE instead of the observed 0.4-0.5 ppb (Figure 2). Therefore, given the relative lower concentrations of PAN in the free troposphere and lower stratosphere and the rapid thermal decomposition, it is unlikely that over 0.4 ppb of PAN could be observed in surface air significantly impacted by stratosphere intrusion, not to mention that the PAN values during the NOE were even much higher than the nighttime values of other dates.

To include our major points on this issue, we extended the discussion in section 3.7 in the revised manuscript on the PAN and O₃ measurement from the ZB supersite:

“To further understand the source characteristic of NOE, the hourly average concentrations of surface PAN and O₃ observed at the ZB supersite are displayed in Figure 2. It can be seen that the variations of PAN and O₃ were in phase and the concentrations of both gases were well correlated ($r^2=0.60$, $p<0.0001$, $n=283$), indicating that the variations of PAN and O₃ were driven mainly by chemical and physical processes within the boundary layer. The maximum O₃ from 02:00 LT to 05:00 LT on 1 August was 88 ± 5 ppbv, matching with PAN of 0.44 ± 0.02 ppbv, which was still significantly higher than those lowest values in nighttime of other dates. As a secondary photochemical pollutant, PAN is thermally unstable but can be transported over higher altitudes, where it has much longer lifetime due to low temperatures. However, observations over the years on mountain tops, aircrafts and satellites showed that the mixing ratios of PAN in the free troposphere and lower stratosphere of the Northern Hemisphere were normally much lower than 0.5 ppb and mostly lower than 0.3 ppb (Singh et al., 2007; Moore and Remedios, 2010; Roiger et al., 2011; Pandey Deolal et al., 2013; Fadnavis et al., 2014; Kramer et al., 2015). PAN decomposes rapidly in warm urban air. According to Cox and Roffey (1977), the lifetime of PAN was only 2.7 hours at 25 °C. In our case, the nighttime temperature at the ZB supersite varied from 33.1 °C at 18:00 LT on 31 July to 20.4 °C at 06:00 LT on 1 August, 2021, with an average of 26.0 °C. Under such warm condition, the thermal decomposition lifetimes were in the range of 0.2-1.3 hours based on the hourly observations. If the surface layer had been significantly impacted by air masses from the free troposphere and lower stratosphere, we would have seen much lower levels of PAN during the NOE instead of the observed 0.4-0.5 ppb (Figure 2). Therefore, given the relative lower concentrations of PAN in the free troposphere and lower stratosphere and the rapid thermal decomposition, it is unlikely that over 0.4 ppb of PAN could be observed in surface air significantly impacted by stratospheric intrusion, not to mention that the PAN values during the NOE were even much higher than the nighttime values before and after the NOE event.”

- Lastly, the authors mention that HOLWCO could also occur in photochemically aged air, not necessarily from STT, but the photochemical age analysis in the manuscript

shows fresh air with ages less than 10 hrs. Does that mean HOLWCO can occur in fresh air as well?

Response: Chen et al. (2022) attributed the ozone-rich and CO-poor phenomenon during the NOE to the downward transport of stratospheric air. In our manuscript we mentioned "photochemically aged pollution air masses may also show HOLWCO features as observed in the PEM-West A campaign (Newell et al. 1996b; Stoller et al., 1999)" and "air mass with HOLWCO feature in free troposphere do not necessarily mean that the O₃ enhancement is originated from the stratosphere (Stoller et al., 1999)". Since HOLWCO phenomena may not be caused by STT, we suggest that more cautions should be taken when attributing HOLWCO events at low altitude sites to stratospheric impact.

The reviewer is asking the possibility of HOLWCO occurring in fresh air, referring the relatively shorter lifetimes we estimated. Our results can neither confirm nor exclude this possibility. Our estimates of photochemical age indicate that surface air at ZB during the NOE was nearly as fresh as at other nights, against a significant impact of stratospheric air, which has ages of years. In addition, the HOLWCO feature during the NOE was very much far from the stratospheric characteristics. The maximum O₃ levels were around 80 ppb and significantly lower than respective daytime maxima; the CO levels were between 200 and 500 ppb (see Figure 3 in Chen et al., 2022 and Figure R4), much higher than the CO levels in the middle and upper troposphere (about 100 ppb) and lower stratosphere (<50 ppb) (Inness et al., 2022) and even not lower than those CO values on some other days; the measured water vapor pressure during the NOE was close to its normal values (Figure R4) and did not show any sign of substantial stratospheric impact. In other words, although the levels of CO or water vapor were relatively lower during the NOE event, they did not show deviations from their values within normal boundary layer, nor substantial STT influences. All these, together with our evidence given above, indicate that the NOE reported in Chen et al. (2022) was not caused by typhoon-induced stratospheric intrusion.

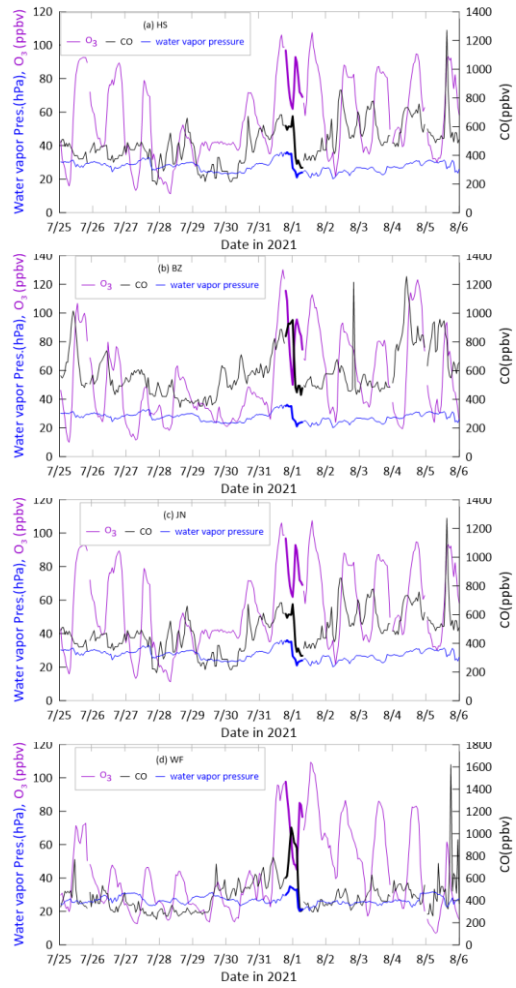


Figure R4. Time series of hourly multi-sites-averages of O₃ (purple), CO (black) and water vapor pressure (blue) between 25 July and 5 August 2021. Data from 18:00 LT on 31 July to 06:00 LT on 1 August are highlighted in thick lines. The multi-site data from HS (4 sites) (a), BZ (6 sites) (b), JN (13 sites) (c), WF (6 sites) (d), QD (13 sites) (e), WH (5 sites) (f) and ZB (7 sites) (g) are available at <https://quotsoft.net/air> (last access: 15 April 2023; X. L. Wang, 2020). Data from the ZB supersite (h) is provided by the Chinese Academy of Environmental Sciences (CRAES). Water vapor pressure data are from <https://data.cma.cn/>.

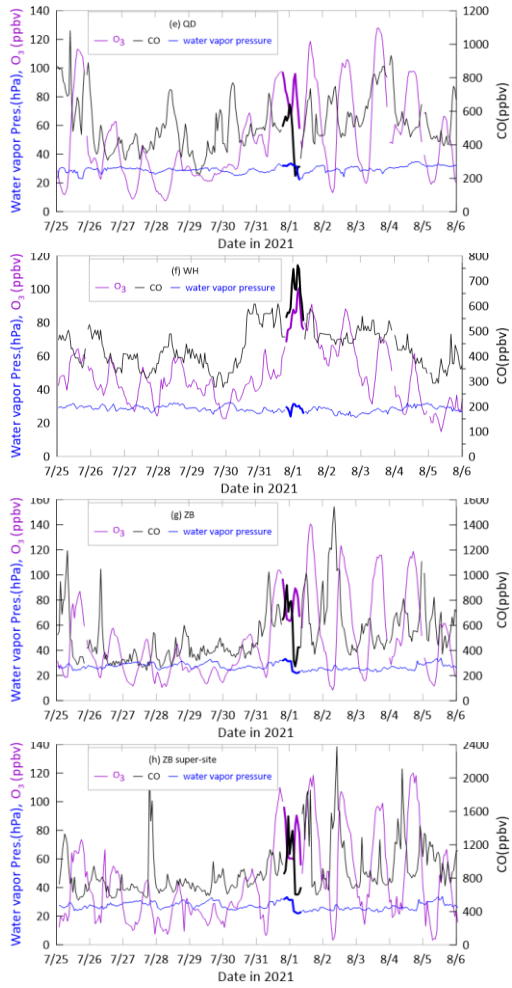


Figure R4. (continued).

We included Figure R4 in the revised supplement as Figure S6 and added some text in section 4 in the revised manuscript to cite and discuss the data in this figure:

“In the NOE cases reported in Chen et al. (2022), the HOLWCO feature during the NOE was very much far from the stratospheric characteristics. The maximum O₃ levels were around 80 ppb and significantly lower than respective daytime maxima; the CO levels were between 200 and 500 ppb (see Figure 3 in Chen et al., 2022 and Figure S6), much higher than the CO levels in the middle and upper troposphere (about 100 ppb) and lower stratosphere (<50 ppb) (Inness et al., 2022) and even not lower than those CO values on some other days; the measured water vapor pressure during the NOE was close to its normal values (Figure S6) and did not show any sign of substantial stratospheric impact. In other words, although the levels of CO or water vapor were relatively lower during the NOE events, they did not show large deviations from their values within normal boundary layer, nor substantial STT influences. All these, together with our evidence given above, indicate that the NOE reported in Chen et al. (2022) was not caused by typhoon-induced stratospheric intrusion. Therefore, more cautions should be taken when attributing HOLWCO events at low altitude sites to stratospheric impact, whether or not there was an influence from a typhoon or other synoptic system. It is suggested that if possible, each case should be verified by analyzing both physical and chemical processes before making a

conclusion.”

2. If possible, the vertical profiles of virtual temperature and winds can be added to further support the conclusion that the rapid downward transport of daytime PPO.

Response. There are three routine radiosonde stations in the studied area, i.e., Zhangqiu (ZQ, 117.524 E, 36.713 N), Rongcheng (RC, 122.477 E, 37.173 N) and QD. ZQ is about 52 km east of JN and RC about 56 km southeast of WH. The radiosonde data collected at 19:00 LT, 31 July and 07:00 LT, 1 August 2021 at these sites can be used to get a glimpse of the vertically thermal and dynamical evolutions in the night of 31 July. The raw radiosonde data include temperature, pressure, relative humidity, and wind speed and direction (<https://data.cma.cn/>). We calculated the virtual temperature and equivalent potential temperature(θ_{se}) (Bolton, 1980) and wind shear, $(du/dz)^2$ (Cho et al., 2001). These vertical profiles of these quantities from surface level to 400 hPa are shown in Figure R5. The pronounced decreasing of θ_{se} below 900 hPa over ZQ and QD from 19:00 LT, 31 July to 07:00 LT, 1 August indicated a descending process occurred at the night. The wind shear peaked near 900 hPa over ZQ and QD, providing kinetic energy for the mixing process. The above thermal and dynamical conditions were, of course, favorable for the downward mixing of higher levels of O₃ in the residual layer over ZQ and QD. Over RC, however, the thermal and dynamical conditions were different (Figure R5c) and less favorable for triggering the downward transport. This is consistent with the data from the neighboring coast city WH, showing high surface O₃ during the NOE event accompanied with relatively high CO and water vapor (Figure R4f).

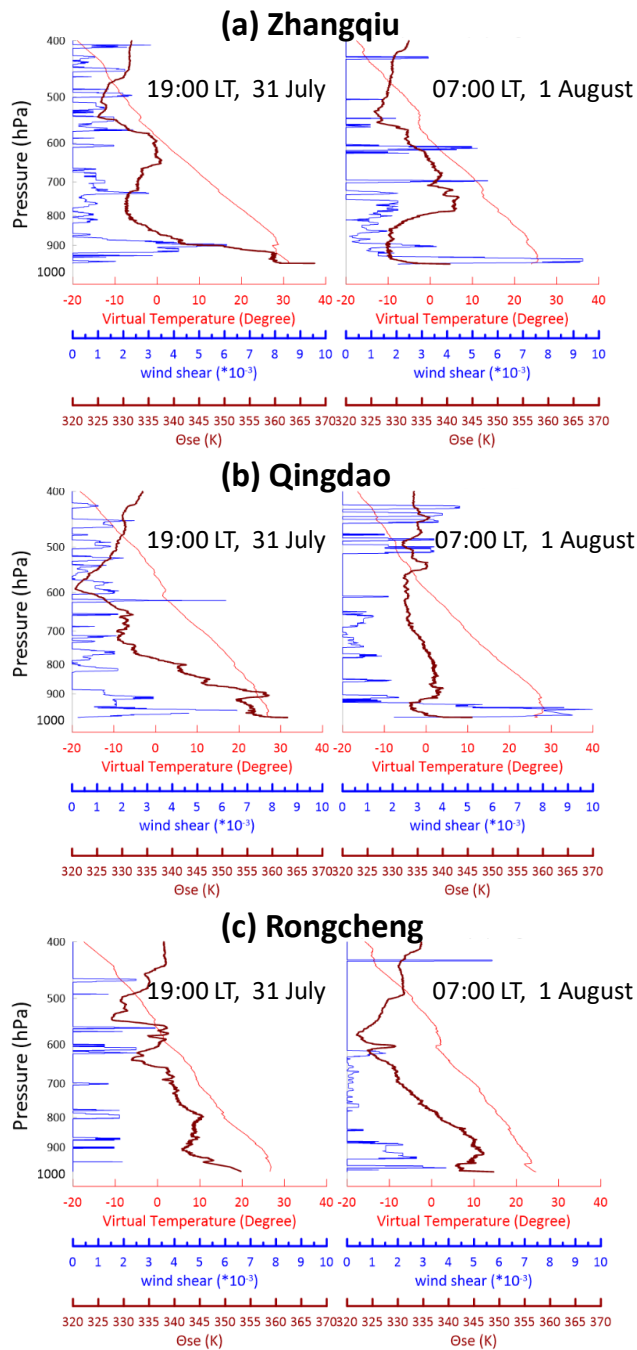


Figure R5. The vertical profiles of virtual temperature (red), equivalent potential temperature (θ_{se} , grey) and wind shear (blue) calculated on the basis of routine radiosonde observations data at 19:00 LT, 31 July and 07:00 LT, 1 August 2021 in Zhangqiu (ZQ)(a), Qingdao (QD)(b) and Rongcheng (RC) (c).

We included Figure R5 in the revised supplement as Figure S5 and added section 3.4 in the revised manuscript to discuss the data in this figure:

“To confirm the possibility of rapid downward transport of daytime PPO, we obtained some radiosonde data from three stations in Shandong Province, i.e., Zhangqiu (ZQ, 117.524 E, 36.713 N), Rongcheng (RC, 122.477 E, 37.173 N) and QD. ZQ is about 52 km east of JN and RC about 56 km southeast of WH. The radiosonde data collected at 19:00 LT, 31 July and 07:00 LT, 1 August 2021 at these sites can be used to get a glimpse of the vertically thermal and dynamical

evolutions in the night of 31 July. The raw radiosonde data include temperature, pressure, relative humidity, and wind speed and direction (<https://data.cma.cn/>). We calculated the virtual temperature and equivalent potential temperature (θ_{se}) (Bolton, 1980) and wind shear, $(du/dz)^2$ (Cho et al., 2001). The vertical profiles of these quantities from surface level to 400 hPa are shown in Figure S5. The pronounced decreasing of θ_{se} below 900 hPa over ZQ and QD from 19:00 LT, 31 July to 07:00 LT, 1 August indicated that a descending process occurred at the night. The wind shear peaked near 900 hPa over ZQ and QD, providing kinetic energy for the mixing process. The above thermal and dynamical conditions were favorable for the downward mixing of higher levels of O_3 in the residual layer over ZQ and QD. Over RC, however, the thermal and dynamical conditions were different (Figure S5c) and less favorable for triggering the downward transport. This is consistent with the data from the neighboring coast city WH, showing high surface O_3 during the NOE event accompanied with relatively high CO and water vapor (Figure S6f). As a coast city near WH, RC should have been impacted by airmasses from marine boundary layer, as discussed for WH in section 3.3.”

Minor Comments:

Line 43: ‘rangeby’ should be ‘range by’.

Response: Thank you. This error was corrected.

Line 66-67: Better to add how many sites there are in each city to the main texts and mention that Fig. 1 is the site average.

Response: Yes, the site numbers were added in the revised manuscript.

“Figure 1: Time series of hourly multi sites-average of O_3 (purple) and NO_2 (bright blue) in several NCP cities between 25 July and 5 August 2021. Data from 18:00 LT on 31 July to 06:00 LT on 1 August are highlighted in red. The multisite data from HS (4 sites) (a), BZ (6 sites) (b), JN (13 sites) (c), WF (6 sites) (d), QD (13 sites) (e), WH (5 sites) (f) and ZB (7 sites) (g) are available at <https://quotsoft.net/air> (last access: 15 April 2023; X. L. Wang, 2020). Data from the ZB supersite (h) is provided by the Chinese Academy of Environmental Sciences (CRAES). The positive (negative) error bars represent one standard deviation of O_3 (NO_2).”

Line 87-90: Consider putting an enlarged figure in the supplement and mark these NOEs. It is hard to identify in Figure 1.

Response : Yes, Figure S2 was included in the revised supplement to show an enlarged view of the NOEs.

Line 127: Change ‘arrived’ to ‘arriving’.

The caption of Figure 3: Change ‘arrived’ to ‘arriving’ and ‘based’ to ‘based on’.

Response : Corrected (line 221).

Reference

Bolton, D .: The computation of equivalent potential temperature, *Mon. Weather Rev.*, **108**, 1046-1053, [https://doi.org/10.1175/1520-0493\(1980\)108<1046:TCOEPT>2.0.CO;2](https://doi.org/10.1175/1520-0493(1980)108<1046:TCOEPT>2.0.CO;2), 1980.

Caputi, D.J., Faloona, I., Trousdale, J., Smoot, J., Falk, N., and Conley, S.: Residual layer ozone, mixing, and the nocturnal jet in California's San Joaquin Valley, *Atmos. Chem. Phys.*, **19**, 4721–4740, <https://doi.org/10.5194/acp-19-4721-2019>, 2019.

Chen, Z., Liu, J., Qie, X., Cheng, X., Shen, Y., Yang, M., Jiang, R., and Liu., X.: Transport of substantial stratospheric ozone to the surface by a dying typhoon and shallow convection, *Atmos. Chem. Phys.*, 22, 8221–8240, <https://doi.org/10.5194/acp-22-8221-2022>, 2022.

Cho, J.Y.N., Newell, R.E., Browell, E.V. , Grant, W.B., Butler, C.F., and Fenn, M.A.: Observation of pollution plume capping by a tropopause fold, *Geophys. Res. Lett.*, 28(17), 3243-3246, <https://doi.org/10.1029/2001GL012898>, 2001.

Cox, R.A. and Roffey, M.J.: Thermal decomposition of peroxyacetyl nitrate in the presence of nitric oxide. *Environ. Sci. Technol.*, 11, 900–906, 1977.

Fadnavis, S., Schultz, M.G., Semeniuk, K., Mahajan, A.S., Pozzoli, L., Sonbawne, S., Ghude, S.D., Kiefer, M., and Eckert, E.: Trends in peroxyacetyl nitrate (PAN) in the upper troposphere and lower stratosphere over southern Asia during the summer monsoon season: regional impacts, *Atmos. Chem. Phys.*, 14, 12725–12743, <https://doi.org/10.5194/acp-14-12725-2014>, 2014.

He, C., Lu, X., Wang, H., Wang, H., Li, Y., He, G., He, Y., Wang, Y., Zhang, Y., Liu, Y., Fan, Q., and Fan, S.: The unexpected high frequency of nocturnal surface ozone enhancement events over China: characteristics and mechanisms, *Atmos. Chem. Phys.*, 22, 15243–15261, <https://doi.org/10.5194/acp-22-15243-2022>, 2022.

Inness, A., Aben, I., Ades, M., Borsdorff, T., Flemming, J., Jones, L., Landgraf, J., Langerock, B., Nedelec, P., Parrington, M., and Ribas, R.: Assimilation of S5P/TROPOMI carbon monoxide data with the global CAMS near-real-time system, *Atmos. Chem. Phys.*, 22, 14355–14376, <https://doi.org/10.5194/acp-22-14355-2022>, 2022.

Kleinman, L., Daum, P., Lee, Y.-N., Nunnermacker, L., Springston, S., Weinstein-Lloyd, J., and Rudolph, J.: Ozone production efficiency in an urban area, *J. Geophys. Res.*, 107, 4733, <https://doi.org/10.1029/2002JD002529>, 2002.

Kley, D., Geiss, H., Mohnen, V.A.: Tropospheric ozone at elevated sites and precursor emissions in the United States and Europe, *Atmos. Environ.*, 28, 149-158, 1994.

Kramer, L.J., Helmig, D., Burkhardt, J.F., Stohl, A., Oltmans, S., and Honrath, R.E.: Seasonal variability of atmospheric nitrogen oxides and non-methane hydrocarbons at the GEOSummit station, Greenland, *Atmos. Chem. Phys.*, 15, 6827–6849, <https://doi.org/10.5194/acp-15-6827-2015>, 2015.

Pandey Deolal, S., Staehelin, J., Brunner, D., Cui, J., Steinbacher, M., Zellweger, C., Henne, S., and Vollmer, M.K.: Transport of PAN and NOy from different source regions to the Swiss high alpine site Jungfraujoch, *Atmos. Environ.*, 64, 103–115, <https://doi.org/10.1016/j.atmosenv.2012.08.021>, 2013.

Roiger, A., Aufmhoff, H., Stock, P., Arnold, F., and Schlager, H.: An aircraft-borne chemical ionization – ion trap mass spectrometer (CI-ITMS) for fast PAN and PPN measurements, *Atmos. Meas. Tech.*, 4, 173–188, <https://doi.org/10.5194/amt-4-173-2011>, 2011.

Rolph, G., Stein, A., and Stunder, B.: Real-time Environmental Applications and Display sYstem: READY. *Environmental Modelling & Software*, 95, 210-228, <https://doi.org/10.1016/j.envsoft.2017.06.025>, 2017.

Singh, H.B., Salas, L., Herlitz, D., Kolyer, R., Czech, E., Avery, M., Crawford, J.H., Pierce, R.B., Sachse, G.W., Blake, D.R., Cohen, R.C., Bertram, T.H., Perring, A., Wooldridge, P.J., Dibb, J., Huey, G., Hudman, R.C., Turquety, S., Emmons, L.K., Flocke, F., Tang, Y.,

Carmichael, G.R., and Horowitz, L.W.: Reactive nitrogen distribution and partitioning in the North American troposphere and lowermost stratosphere, J. Geophys. Res., 112, D12S04, <https://doi.org/10.1029/2006JD007664>, 2007.

Stein, A.F., Draxler, R.R., Rolph, G.D., Stunder, B.J.B., Cohen, M.D., and Ngan, F.: NOAA's HYSPLIT atmospheric transport and dispersion modeling system, Bull. Amer. Meteor. Soc., 96, 2059-2077, <http://dx.doi.org/10.1175/BAMS-D-14-00110.1>, 2015.

Tang, G., Zhu, X., Xin, J., Hu, B., Song, T., Sun, Y., Wang, L., Wu, F., Sun, J., Cheng, M., Chao, N., Li, X., Wang, Y.: Modelling study of boundary-layer ozone over northern China - Part II: Responses to emission reductions during the Beijing Olympics, Atmos. Res., 193, 83–93, <http://dx.doi.org/10.1016/j.atmosres.2017.02.014>, 2017.

Wang, H., Lu, K., Chen, X., Zhu, Q., Wu, Z., Wu, Y., and Sun, K.: Fast particulate nitrate formation via N₂O₅ uptake aloft in winter in Beijing, Atmos. Chem. Phys., 18, 10483–10495, <https://doi.org/10.5194/acp-18-10483-2018>, 2018.

Xu, X., Zhang, H., Lin, W., Wang, Y., Xu, W., and Jia, S.: First simultaneous measurements of peroxyacetyl nitrate (PAN) and ozone at Nam Co in the central Tibetan Plateau: impacts from the PBL evolution and transport processes, Atmos. Chem. Phys., 18, 5199–5217, <https://doi.org/10.5194/acp-18-5199-2018>, 2018.

Response to Reviewer #2:

The study from Zheng et al. is a comment on the study by Chen et al. (2022). Chen et al. (2022) demonstrated that the intrusion of stratosphere ozone induced by Typhoon Infa served as a potential source of surface ozone, and the following shallow local mesoscale convective systems facilitated the downward transport of this potential ozone source to the surface, and led to a nocturnal ozone enhancement (NOE) event in the North China Plain (NCP). Zheng et al. analyzed observations (including PAN, VOCs) from the ZiBo supersite at eastern NCP, and argued that the NOE event originated from fresh ozone photochemical production in the lower troposphere rather than from the stratosphere as pointed out by Chen et al. (2022). This is supported by 1) comparable nighttime surface O_x and daytime O₃ levels, 2) a strong correlation between PAN and ozone during the NOE event, and 3) the short photochemical ages of air mass. Overall, the study provides strong observational evidence on the conclusion, and is well-designed and well-written. I suggest some revisions before publication.

Response: We thank the reviewer for the positive comments.

While I agree with Zheng et al. that the mixing of ozone produced photochemically and stored in the residual layer has a large contribution to the Zibo NOE event, it does not necessarily exclude the possibility of stratospheric contribution proposed by Chen et al. (2022). Zheng et al. mainly used observations at ZiBo city, however, as seen from Figure 8 of Chen et al. (2022), there is limited vertical atmospheric activity near the ZiBo supersite, as the main convective zone is located in the western Shandong Province. So the difference in the study region between Chen et al. (2022) and Zheng et al. may also contribute to the different conclusions. I would suggest the authors consider this point in their analysis.

Response: Indeed, Figure 8 of Chen et al. (2022) indicates that the vertical atmospheric activity seemed to be limited near Zibo and the main convective zone was in the western Shandong Province. However, this figure presents by far not the

whole process of the convective activity because it only show six snapshots of the mesoscale convective system (MSC) observed between 20:00 LT, 31 July and 01:00 LT, 1 August 2021 and does not show the dissipation of the MSC. The radar reflectivity maps in Figure R6 add additional snapshots to the MSC. As can be seen in Figures R6b-R6f, Zibo and Jinan were clearly under the influence of the MSC around 00:00 LT, hited heavily by the MSC between 01:00 LT and 03:00 LT, 1 August. Without doubt, the MSC impacting the cities with NOEs reported in Chen et al. (2022) also impacted Zibo. The radar reflectivity maps show clearly that except QD and WH, all cities listed in our Table 1 were strongly impacted by the MSC. While the occurrence of the NOE was a little later than the MSC impact, the sequence of the MSC impacts is consistent with that of the NOE events. Therefore, the major conclusions based on our analysis apply also to Chen et al. (2022).

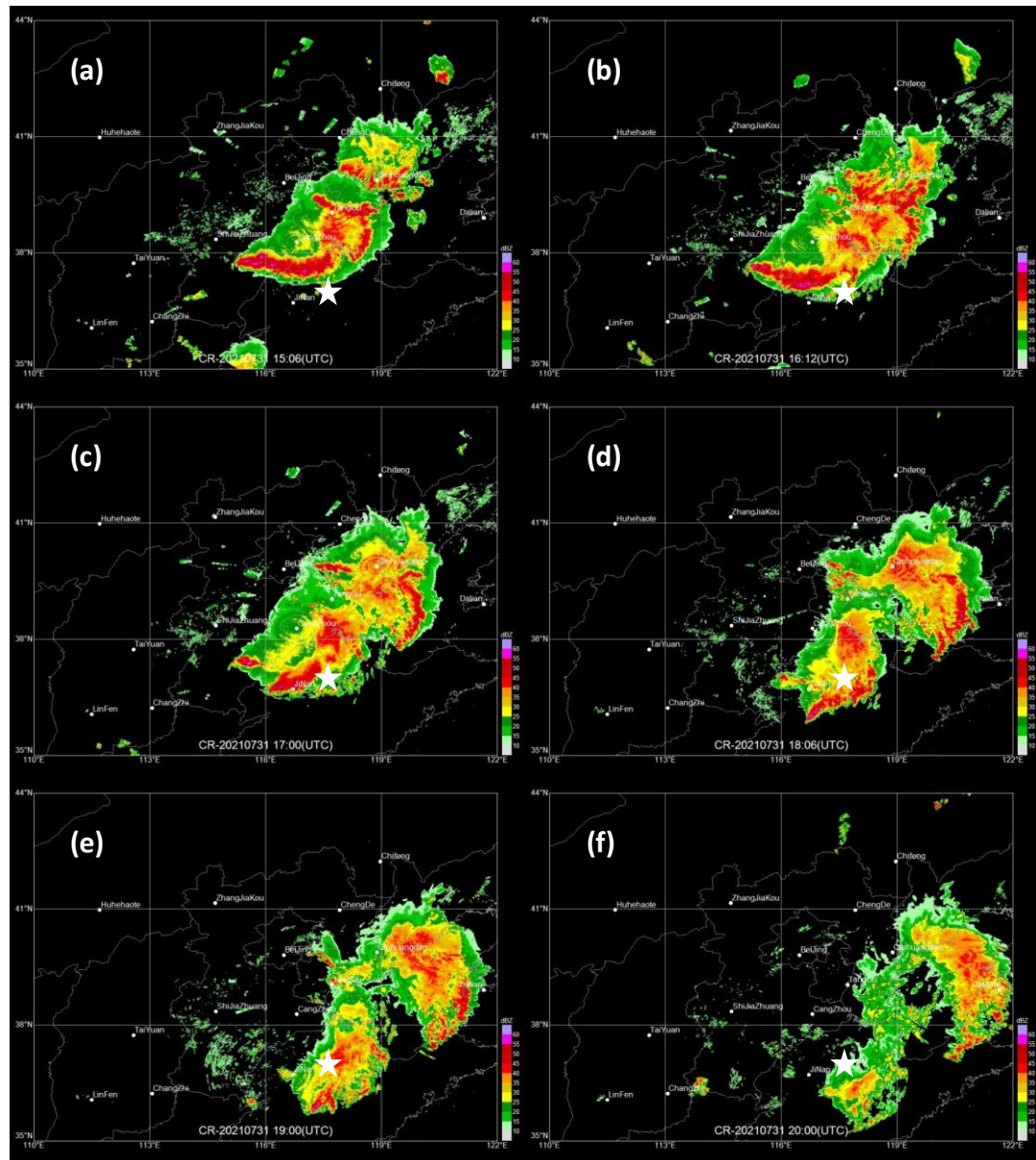


Figure R6. Radar reflectivity maps for the North China Plain at (a) 15:06 UTC (23:00 LT, 31 July), (b) 16:12 UTC (00:12 LT, 1 August), (c) 17:00 UTC (01:00 LT, 1 August), (d) 18:06 UTC (02:06 LT, 1 August),

(e) 19:00 UTC (03:00 LT, 1 August) and (f) 20:00 UTC (04:00 LT, 1 August). Some of the major cities are indicated on the maps. The white star on each map shows the location of Zibo.

We included Figure R6 in the revised supplement as Figure S7 and added section 3.5 in the revised manuscript to discuss this issue:

“Above analyses show that not all cities in the study area were clearly influenced by strong downward transport. The cities strongly impacted by the MCSs should have experienced intensive vertical air motion. Chen et al. (2022) showed in their Figure 8 that the vertical atmospheric activity seemed to be limited near ZB and the main convective zone was in the western Shandong Province. However, this figure presents by far not the whole process of the convective activity because it only show six snapshots of the MSCs observed between 20:00 LT, 31 July and 01:00 LT, 1 August 2021 and does not show the dissipation of the MSCs. The radar reflectivity maps in Figure S7 add additional snapshots to the MSCs. As can be seen in Figure S7b-f, ZB and JN were clearly under the influence of the MSCs around 00:00 LT, hit heavily by the MSCs between 01:00 LT and 03:00 LT, 1 August. Without doubt, the MSCs impacting the cities with NOEs reported in Chen et al. (2022) also impacted ZB. The radar reflectivity maps show clearly that except QD and WH, all cities listed in our Table 1 were strongly impacted by the MSCs. While the occurrence of the NOE was a little later than the MSCs impact, the sequence of the MSCs impacts is consistent with that of the NOE events. Therefore, the major conclusions based on our analysis of data from the ZB supersite should also apply to Chen et al. (2022). In next sections, we offer more evidence from ZB to support our argument.”

One small comment is to clarify O_3 as “daytime O_3 ” and O_x as “nighttime O_x ” in Table 1

Response: Thank you. We added clarifications in the revised manuscript and supplement.

We included the discussion about the comparison between afternoon O_3 and O_x in the NBL in the revised supplement as Text S1 (lines 77-122), changed the original Text S1 to Text S2 and renumbered the equations and figures.

“Text S1 Identifying potential origin of the NOE by comparing afternoon O_3 with O_x in the NBL during the NOE

Our intention is to check whether or not surface O_3 observed during the NOE contained significant contribution of O_3 from the stratosphere. For this purpose, a comparison of O_3 levels in the vertical direction is helpful.In summary, $[O_x]_{NBL}$ should be significantly higher than $[O_3]_{aft}$ if the NBL is really impacted by stratospheric O_3 , otherwise the STT impact is negligible even though a NOE event is observed.”

In section 3.2 in the revised manuscript, we cited Text S1 and changed text as follows:

“Following the method of He et al. (2022), we make comparison of O_3 averages during 14:00-17:00 LT on 31 July in the above cities with the respective O_x (O_3+NO_2) averages during the periods of the maximum NOE between 31 July and 1 August (Table 1). Such comparison facilitates the judgement whether or not the NOE was caused by downward mixing of air in the

residual layer (RL) into the nocturnal boundary layer (NBL) because afternoon averages of O_3 in the convective boundary layer are well preserved at night in the RL and O_x is a more conserved quantity than O_3 in the NBL. Details about the reasonability of this method are given in Text S1. It can be seen in Table 1 that, except for WH, the nighttime O_x averages approach to or obviously lower than the respective daytime O_3 averages. In the mega-cities QD and JN, the average levels of O_x during the maximum NOE were nearly the same as those of daytime O_3 , while the nighttime O_x in the other cities (excluding WH) was at least a few ppbv lower than daytime O_3 . According to the discussions in Text S1, for all cities excluding WH, data in Table 1 do not suggest any significant STT impact on the NOE events.”

In addition to above changes, we made minor changes in abstract, added references cited in the reference lists, modified Figure 1 by showing only one side error-bars and corrected any errors we found. Please see more details in our marked-up manuscript and supplement.

Comment on “Transport of substantial stratospheric ozone to the surface by a dying typhoon and shallow convection” by Chen et al. (2022)

Xiangdong Zheng¹, Wen Yang², Yuting Sun^{1,3}, Chunmei Geng², Yingying Liu², Xiaobin Xu¹

5 | ¹~~Key Laboratory for Atmospheric Chemistry of CMA & Institute of the Tibet Plateau~~, Chinese Academy of Meteorological Sciences, Beijing 100081, China

²State Key Laboratory of Environmental Criteria and Risk Assessment, Chinese Research Academy of Environmental Sciences, Beijing 100012, China

³Nanjing University of Information Science & Technology, Nanjing, Jiangsu, 210044, China

10 *Correspondence to:* Xiaobin Xu (xiaobin_xu@189.cn)

Abstract. Chen et al. (2022) analyzed the event of rapid nocturnal O₃ enhancement (NOE) observed on 31 July 2021 at surface level in the North China Plain and proposed transport of substantial stratosphere ozone to the surface by Typhoon In-fa followed by downdraft of shallow convection as the mechanism of the NOE event. The analysis seems to be valid in the view-point of atmospheric physics. This comment revisits the NOE phenomenon on the basis of the China National

15 Environmental Monitoring Center (CNEMC) network data ever used in Chen et al. (2022), together with the CNEMC data from Zibo (ZB), and O₃, NO_x, PAN ([peroxyacetic nitric anhydride](#)) and VOCs ([volatile organic compounds](#)) data from the Zibo supersite operated by China Research Academy of Environmental Sciences (CRAES). We found (a) O_x (O₃+NO₂) levels during the NOE period approaching to those of O₃ during 14:00-17:00 LT; (b) the [levels of PAN and the relationship between O₃ and PAN](#) ([peroxyacetic nitric anhydride](#)) consistent with dominance of chemical and physical processes within the boundary layer, and (c) estimated photochemical ages of air mass being shorter than one day and showing no drastic increases during the NOE. We argue that the NOE was not caused by typhoon-induced stratospheric intrusion but originated from fresh photochemical production in the lower troposphere. [Our argument is well supported by the analysis of atmospheric transport as well as ground-based remote sensing data.](#)

1 Introduction

25 Chen et al. (2022) reported a phenomenon of rapid nocturnal ozone (O₃) enhancement (NOE) occurred at the surface level during the night of 31 July 2021 in six cities in the North China Plain (NCP, 34-40 °N, 114-121 °E). Prior to the NOE, the NCP was impacted by Typhoon In-fa, which was largely weakened by 30 July 2021. The mesoscale convective systems (MCSs) formed and passed through the NCP at night on 31 July 2021. Chen et al. (2022) concluded that the NOE phenomenon resulted from "the direct stratospheric intrusion to reach the surface" and was "induced by the multi-scale 30 interactions between the dying Typhoon In-fa and local MCSs". The study suggested that the dying Typhoon In-fa induced

stratospheric troposphere transport (STT) of O_3 followed by downdrafts of shallow convections, which resulted in "transport of substantial stratospheric ozone to the surface". The relatively high O_3 -low water vapor and CO (HOLWCO) concentrations observed at some sites in the NCP and the relative variations of water vapor, O_3 profiles respectively from radiosonde data and the AIRS satellite product were used to support the conclusions.

35 STT processes are triggered by the large-scale circulation or synoptic-scale dynamical processes (Holton et al., 1995). A global study (Škerlak et al., 2014) shows that STT displays strong regional distribution and seasonal variations, and the NCP is not a hot region particularly in summer. STT can be an important source of tropospheric O_3 , particularly in regions where the photochemistry is weak (Lelieveld and Dentner, 2000). However, tropospheric O_3 originates dominantly from photochemistry within the troposphere and photochemically produced O_3 (PPO) is the more important O_3 source not only in 40 the middle-low troposphere (Lelieveld and Dentener, 2000; Logan, 1985) but also in the upper troposphere (Chameides, 1978; Liu et al., 1983; Jaeglé et al., 1998). Anthropogenic and natural O_3 precursors convectively transported from the surface or lower troposphere and lightning produced NO_x may involve PPO in the upper troposphere. Precursors emitted near the surface contribute largely to PPO in the surface and boundary layer, which can be transported upwards through the 45 warm conveyor belt (Bethan et al., 1998; Cooper et al., 2002), spread in the free atmosphere and delivered over a long range by atmospheric circulations (Parrish et al., 1998). PPO in the surface boundary layer is mainly removed by NO_x titration reactions and dry deposition. The NCP is a hot region of PPO from the surface level up to 2.5 km in the summer (e.g., Ding et al., 2008) and has demonstrated rapid long-term increases in surface O_3 levels (Ma et al., 2016; Lu et al., 2018; Lyu et al., 2023).

50 Typhoons are tropical cyclones formed over the western North Pacific regions, which have well-organized structures of updrafts and downdrafts over hundreds and thousands of kilometres (Ahrens and Henson, 2016). A large-scale tropical cyclone with well self-organized character is able to induce dynamical processes and form an outflow layer in the upper troposphere and lower stratosphere (UTLS) and cause strong downdrafts in the periphery of the cyclone (Merrill, 1988; Ahrens and Henson, 2016). The strong air subsidence in the periphery of a typhoon can theoretically lead to the STT of O_3 . It 55 was suggested that the observed enhancement of O_3 in the middle troposphere over the Indian Ocean was caused by the STT through ageostrophic process linked to the strong tropical cyclone Marlene, which occurred in April 1995 (Baray et al., 1999). This suggestion is supported by a modeling study (de Bellevue et al., 2007). However, the idea that O_3 increases in the mid- and upper-troposphere are directly from the STT processes induced by typhoons is less supported by in-situ aircraft-borne observations by Cario et al. (2008) and the literature reviewed therein. Especially, the comparative studies on the Supertyphoon Mireille (1991) during the Pacific Exploratory Mission(PEM)-West A campaign (Newell et al., 1996a; 60 Preston et al., 2019) and the Hurricanes Floyd (1999) and Georges (1998) in the Atlantic Ocean during their phases of intensification and weakening (Carsey and Willoughby, 2005) provided little evidence of the STT of O_3 . On the other hand, the analysis of ERA5 PV (potential vorticity) and air mass with HOLWCO observed below 12 km by the In-service Aircraft for a Global Observing System (IGOS) indicated the occurrence of STT induced by typhoons (Roux et al., 2020; Z. Chen et al., 2021). However, it should be noted that atmospheric large-scale subsidence over East Asia can also be induced by the

65 strong summer subtropical high. Photochemically aged pollution air masses may also show HOLWCO features as observed in the PEM-West A campaign (Newell et al. 1996b; Stoller et al., 1999).

2 Data

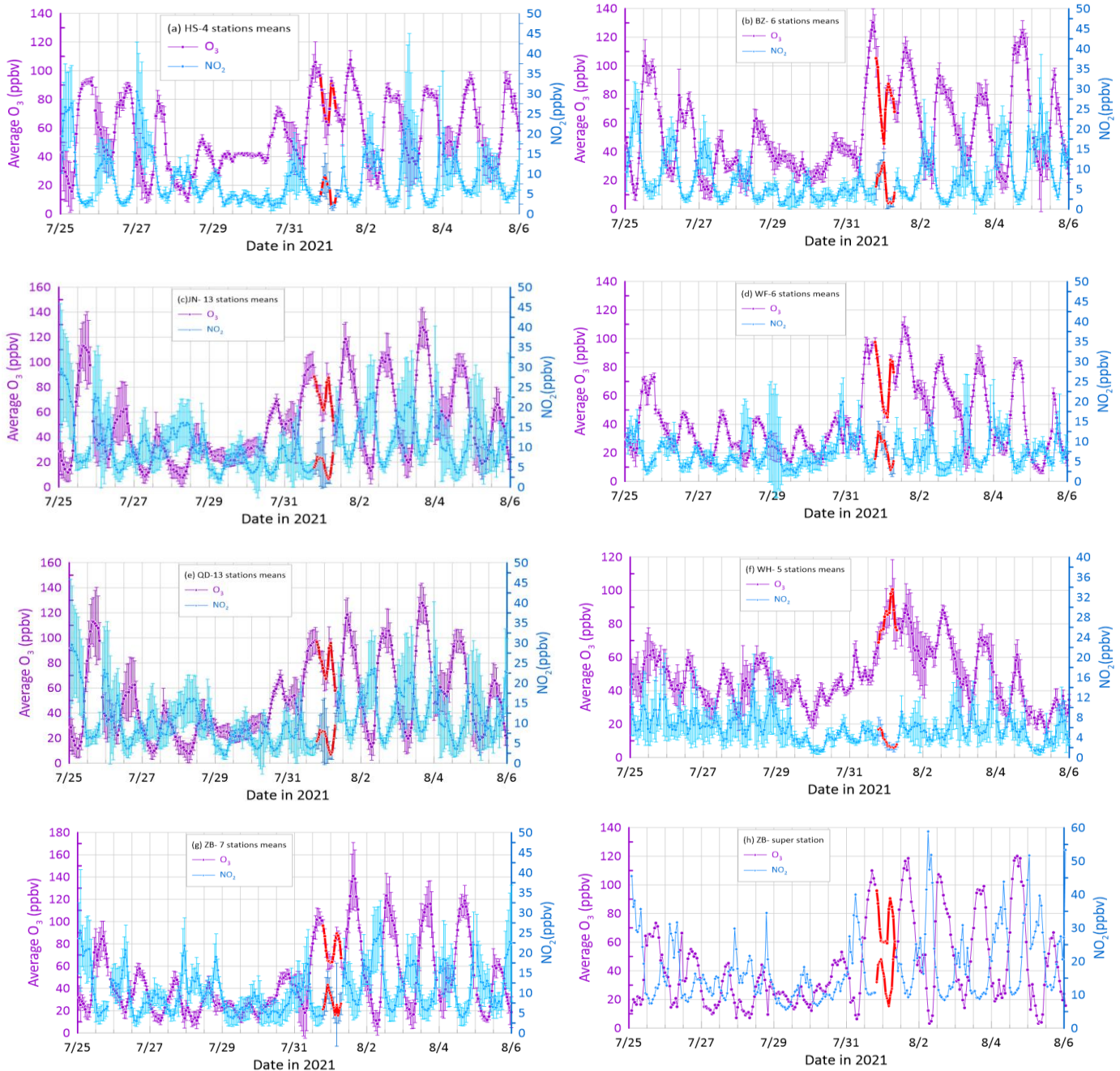
Surface O₃, NO_x, and meteorology data collected in the cities Hengshui (HS), Binzhou (BZ), Jinan (JN), Weifang (WF), 70 Qingdao (QD), Weihai (WH) and the newly added Zibo (ZB) were from the China National Environmental Monitoring Center (CNEMC) network (<https://quotsoft.net/air>). The geographical location of ZB is shown in Figure S1. In addition, hourly averages of surface O₃, PAN ([peroxyacetic nitric anhydride](#)), NO_x, and VOCs ([volatile organic compounds](#)) were obtained from a supersite in ZB, operated by China Research Academy of Environmental Sciences (CRAES). Ambient O₃ and NO_x at the supersite were monitored using a Model 49i ozone analyzer and a Model 42i NO/NO₂/NO_x analyzer (both from Thermo Fischer Scientific), respectively. The analyzers were calibrated weekly. Quasi-continuous measurement of 75 PAN was made using a gas chromatograph coupled with an electron capture detector (GC-ECD) (ZC-PANs, Research Center for Eco-Environmental Sciences, Chinese Academy of Sciences). The GC-ECD system was calibrated seasonally using PAN inline produced from CH₃COCH₃+NO reactions under UV irradiation (J. Chen et al., 2021). Samples of VOCs were taken hourly and analyzed using a coupled gas chromatograph-mass spectrometry (GC-MS) system (5800-GM, Thermo Fischer Scientific), which was calibrated monthly using standard gas mixture from Linda, containing 116 species 80 including hydrocarbons, oxygenated and halogenated hydrocarbons.

3 Verification of results in Chen et al. (2022)

3.1 [Summary of observed NOE events](#)

The hourly averages of surface O₃ and NO_x in the six cities (HS, BZ, JN, WF, QD, and WH) listed in Chen et al., (2022) as well as those from ZB and the ZB supersite are shown in Figure 1. The data of O₃ and NO_x from 18:00 LT on 31 July to 85 06:00 LT on 1 August 2021 are highlighted in red lines [in Figures 1 and 2S](#). Although PPO was not obvious during 29-30 July due to the weather conditions, the diurnal variations of O₃ and NO_x on most days displayed typical features being controlled by the PPO process, with O₃ maxima and correspondingly NO_x minima during 14:00~17:00 and rapid nighttime 90 O₃ decreases due to substantial NO_x titration reactions [and dry deposition](#). As reported by Chen et al. (2022), a clear NOE was observed during the night of 31 July in HS, BZ, JN, WF, and QD. Our data from ZB (Figures [1g](#) and [4h](#)) also confirm the occurrence of this NOE. However, it is noteworthy that NOE events occurred not only during the night of 31 July but also during some other nights in these cities with O₃ enhancement of 5-20 ppbv. The frequency of NOE was highest in WH, in details: O₃ increased from 24±8 ppbv at 22:00 LT on 27 July to 46±21 ppbv at 01:00 LT on 28 July; from 23±5 ppbv at 23:00 LT on 29 July to 40±4 ppbv at 04:00 LT on 30 July; from 43±2 ppbv at 00:00 LT to 57±3 ppbv at 04:00 LT on 31 July; from 54±19 ppbv at 00:00 LT to 66±5 ppbv at 02:00 LT on 2 August; from 42±17 ppbv at 00:00 LT to 48±5 ppbv at 03:00

95 LT on 3 August; from 20 ± 4 ppbv at 02:00 LT to 25 ± 2 ppbv at 03:00 LT on 5 August. Other NOE events occurred, for example, on 4 August in HS, on 28 July and 5 August in BZ, on 26 July and 4 August in JN, on 4 August in WF and QD.
Therefore, the NOE events occur frequently in the NCP, regardless the impacts from typhoon or STT, as already reported in He et al. (2022).



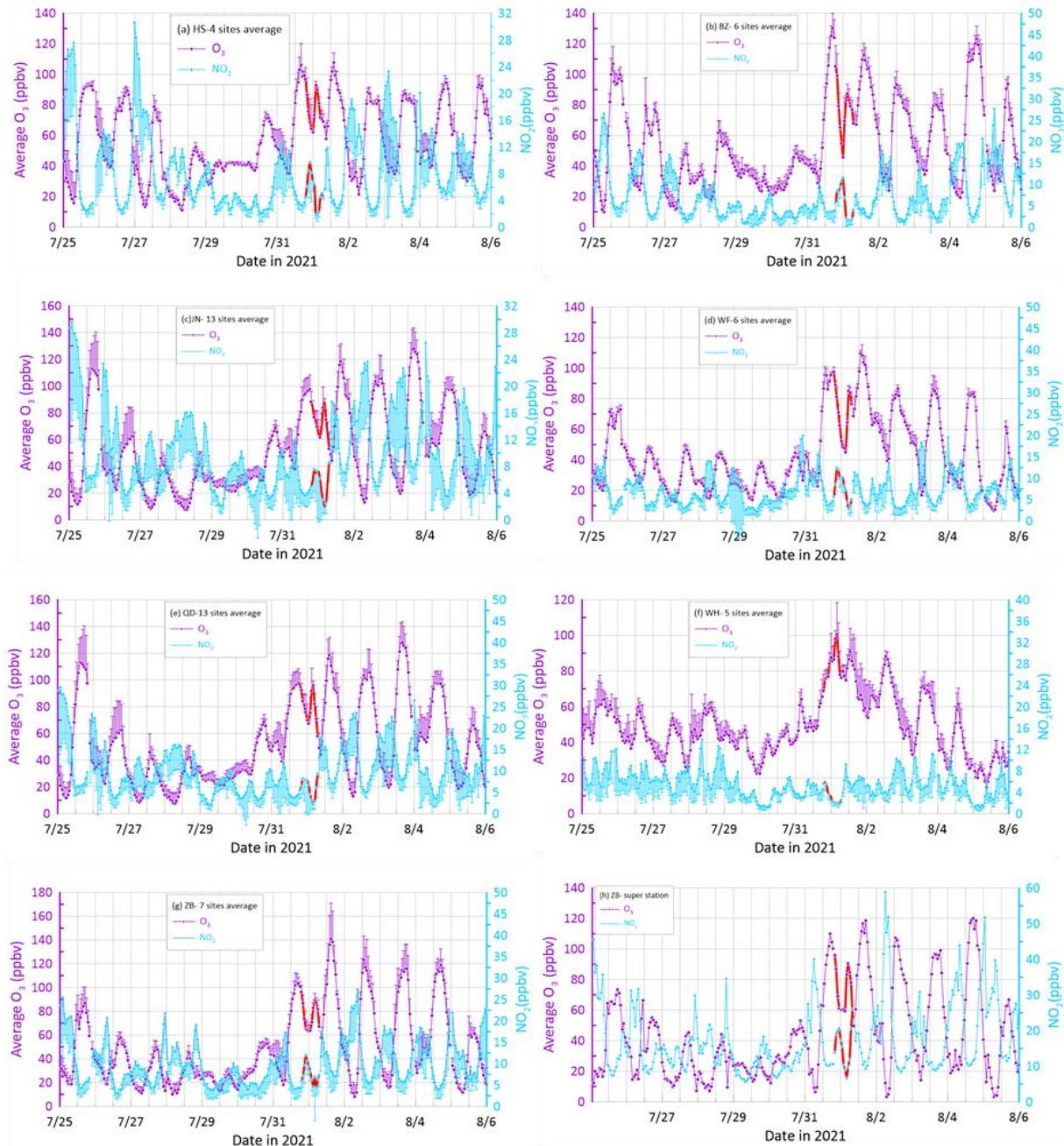


Figure 1: Time series of hourly multi sites-average of O_3 (purple) and NO_x-NO_2 (bright blue) with one standard deviation in several NCP cities between 25 July and 5 August 2021. Data from 18:00 LT on 31 July to 06:00 LT on 1 August are highlighted in

red. The multisite data from HS (4 sites) (a), BZ (6 sites) (b), JN (13 sites) (c), WF (6 sites) (d), QD (13 sites) (e), WH (5 sites) (f) and ZB (7 sites) (g) are available at <https://quotsoft.net/air> (last access: 15 April 2023; X. L. Wang, 2020). Data from the ZB supersite (h) is provided by the Chinese Academy of Environmental Sciences (CRAES). The positive (negative) error bars represent one standard deviation of O_3 (NO_2).

3.2 Identifying the origin of the NOE by comparing afternoon O_3 with O_x in the NBL

Following the method of He et al. (2022), we make comparison of O_3 averages during 14:00-17:00 LT on 31 July in the above cities with the respective O_x (O_3+NO_2) averages during the periods of the maximum NOE between 31 July and 1 August (Table 1). Such comparison facilitates the judgement whether or not the NOE was caused by downward mixing of air in the residual layer (RL) into the nocturnal boundary layer (NBL) because afternoon averages of O_3 in the convective boundary layer are well preserved at night in the RL and O_x is a more conserved quantity than O_3 in the NBL. Details about the reasonability of this method are given in Text S1. It can be seen in Table 1 that, except for WH, the nighttime O_x averages approach to or obviously lower than the respective daytime O_3 averages. In the mega-cities QD and JN, the average levels of O_x during the maximum NOE were nearly the same as those of daytime O_3 , while the nighttime O_x in the other cities (excluding WH) was at least a few ppbv lower than daytime O_3 . According to the discussions in Text S1, for all cities excluding WH, data in Table 1 do not suggest any significant STT impact on the NOE events.

Table 1: Averages of surface O_3 during 14:00-17:00 LT and O_x during the periods of the maximum NOE in the night from 31 July to 1 August 2021.

Cities	NOE time	Daytime mean $O_3 \pm std$ (ppbv)	Nighttime mean $O_x \pm std$ (ppbv)
HS (4 sites)	01:00-02:00	101.7 \pm 3.5	93.1 \pm 2.2
BZ(6 sites)	01:00-03:00	124.1 \pm 5.4	94.6 \pm 2.3
JN(13 sites)	02:00-03:00	96.1 \pm 1.6	96.6 \pm 2.2
WF(6 sites)	04:00-05:00	92.5 \pm 4.8	88 \pm 0.3
QD(13 sites)	02:00-03:00	96.1 \pm 1.6	96.6 \pm 2.2
WH(5 sites)	02:00-03:00	59.2 \pm 7.1	101.3 \pm 1.9
ZB(7 sites)	02:00-05:00	102.6 \pm 1.4	90.9 \pm 4.2
ZB-Supersite	02:00-05:00	104.2 \pm 4.3	93.8 \pm 3.0

3.3 Analysis of atmospheric transport

130 The case of WH deserves more detailed analysis. WH is a relatively smaller city in the tip of the Shandong Peninsula. The higher O_x concentration for WH in Table 1 was probably related to the regional transport of air pollution and the influence of the diurnal alternations of land-sea breezes. Actually, the afternoon PPO in WH had not been well established as shown in Figure 1f. During the daytime (particularly afternoon), when sea breeze dominates, PPO is significantly diluted by cleaner air from the marine boundary layer. The daily maximum of O₃ in WH is generally observed between 11:00 LT and 13:00 LT, rather than between 14:00 LT and 17:00 LT. If the O₃ average for WH in Table 1 were replaced with that from 11:00 LT to 13:00 LT on 1 August (80 ± 2.0 ppbv), then the difference between O_x and O₃ would be reduced to about 21 only 13.00 ppbv.

135 At night, when the land breeze dominates, the near surface level of WH is usually controlled by divergence, which induces downdraft from the residual layer, transports daytime PPO residing in the residual layer to the surface, and resulted in the NOE. This is might have been the main reason of highly frequent NOE emerging in WH.

140 Chen et al. (2022) investigated the atmospheric transport process of the NOE by using high-resolution Weather Research and Forecasting (WRF) simulation and FLEXible PARTicle (FLEXPART) particle dispersion modelling. They presented the two scenarios for BZ and QD and found very different results for the two cities. To support above view, we calculated backward trajectories of air parcels arriving at 100 m above ground level over WH every hour between 19:00 and 08:00 UTC, 31 July 2021 using HYSPLIT model (<https://www.ready.noaa.gov/HYSPLIT.php>) and the Global Forecast System (GFS) reanalysis data (0.25 ° resolution, https://www.emc.ncep.noaa.gov/emc/pages/numerical_forecast_systems/gfs.php).

145 Our intention is not to resolve the dynamical evolution of the MCSs but to analyze atmospheric transport at a relatively larger scale. Figure S3 shows the calculated backward trajectories for WH, together with those for ZB and BZ in the same time window. The trajectories in Figure S3(right) indicate that air parcels influencing the NBL in WH were mostly from the marine boundary layer over the Yellow Sea area. The prevailing wind direction at 850 hPa over the Yellow Sea and the neighbouring land was SW, as shown in Figure 5a in Chen et al. (2022). Such wind condition could facilitate the transport of PPO from the continent to the sea area. Because of the lower emissions of NO_x over the sea, PPO can be well sustained at night and transported to continental locations like WH through sea breezes.

150 The 24-h backward trajectories for ZB (Figure S3(left)) and BZ (Figure S3(middle)) provide additional clues denying STT impacts on nighttime O₃ in these cities. All the trajectories do not indicate any transport of air parcels from altitudes over daytime boundary layer. To gain a more complete insight into the air movements during and before the NOE events, we show in Figure S4 a matrix of backward trajectories for air parcels arriving at 100 m above ground level over the domain 36 °38' N and 115 °122' E at 19:00 UTC (03:00 LT), 31 July 2021. The trajectory heights and locations shown in Figure S4 indicate that only 3 of the 24 trajectories travelled over daytime boundary layer and the 3 trajectories ended at locations over the Bohai Gulf. Therefore, our systematic trajectory analysis does not suggest that the NOE events in the NCP cities were related with downward transport of airmasses from the free troposphere.

3.4 Confirming rapid downward transport of daytime PPO

To confirm the possibility of rapid downward transport of daytime PPO, we obtained some radiosonde data from three stations in Shandong Province, i.e., Zhangqiu (ZQ, 117.524 E, 36.713 N), Rongcheng (RC, 122.477 E, 37.173 N) and QD. ZQ is about 52 km east of JN and RC about 56 km southeast of WH. The radiosonde data collected at 19:00 LT, 31 July and 07:00 LT, 1 August 2021 at these sites can be used to get a glimpse of the vertically thermal and dynamical evolutions in the night of 31 July. The raw radiosonde data include temperature, pressure, relative humidity, and wind speed and direction (<https://data.cma.cn/>). We calculated the virtual temperature and equivalent potential temperature (θ_{se}) (Bolton, 1980) and wind shear, $(du/dz)^2$ (Cho et al., 2001). The vertical profiles of these quantities from surface level to 400 hPa are shown in Figure S5. The pronounced decreasing of θ_{se} below 900 hPa over ZQ and QD from 19:00 LT, 31 July to 07:00 LT, 1 August indicated that a descending process occurred at the night. The wind shear peaked near 900 hPa over ZQ and QD, providing kinetic energy for the mixing process. The above thermal and dynamical conditions were favorable for the downward mixing of higher levels of O_3 in the residual layer over ZQ and QD. Over RC, however, the thermal and dynamical conditions were different (Figure S5c) and less favorable for triggering the downward transport. This is consistent with the data from the neighboring coast city WH, showing high surface O_3 during the NOE event accompanied with relatively high CO and water vapor (Figure S6f). As a coast city near WH, RC should have been impacted by airmasses from marine boundary layer, as discussed for WH in section 3.3.

3.5 Cities impacted by the mesoscale convective systems

Above analyses show that not all cities in the study area were clearly influenced by strong downward transport. The cities strongly impacted by the MCSs should have experienced intensive vertical air motion. Chen et al. (2022) showed in their Figure 8 that the vertical atmospheric activity seemed to be limited near ZB and the main convective zone was in the western Shandong Province. However, this figure presents by far not the whole process of the convective activity because it only show six snapshots of the MCSs observed between 20:00 LT, 31 July and 01:00 LT, 1 August 2021 and does not show the dissipation of the MCSs. The radar reflectivity maps in Figure S7 add additional snapshots to the MCSs. As can be seen in Figure S7b-f, ZB and JN were clearly under the influence of the MCSs around 00:00 LT, hit heavily by the MCSs between 01:00 LT and 03:00 LT, 1 August. Without doubt, the MCSs impacting the cities with NOEs reported in Chen et al. (2022) also impacted ZB. The radar reflectivity maps show clearly that except QD and WH, all cities listed in our Table 1 were strongly impacted by the MCSs. While the occurrence of the NOE was a little later than the MCSs impact, the sequence of the MCSs impacts is consistent with that of the NOE events. Therefore, the major conclusions based on our analysis of data from the ZB supersite should also apply to Chen et al. (2022). In next sections, we offer more evidence from ZB to support our argument.

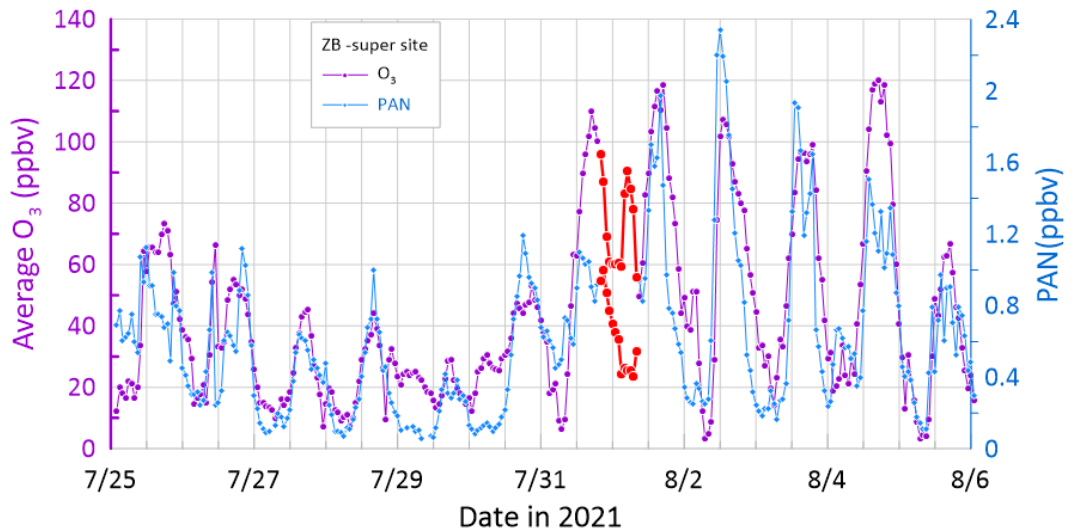
3.6 Evidence from ground-based remote sensing

In addition to the backward trajectories, some ground-based remote sensing data from ZB also support our view. Figure S8 presents time-altitude cross sections of O₃, relative humidity (RH), virtual temperature (Tv) and wind speed (WS) observed at the ZB supersite between 18:00 LT, 31 July and 06:00 LT, 1 August 2021. As can be seen in the figure, relatively higher O₃ mixing ratios occurred only below about 0.5 km. From the evening to midnight, very strong wind prevailed below 1 km, after which humidity was largely enhanced, it rained and the NOE event occurred. The wind directions below 1 km were southerly before 01:00 LT and turned to northerly by 02:00 LT (Figure S9). The top of the higher O₃ layer was partly uplifted during the NOE period. According to the backward trajectories shown in Figure S3(left), the air parcels were from the southwest sector and travelled mostly below 0.5 km above sea level. Both the remote sensing data and the trajectory analysis provide no evidence of air from the free troposphere. Therefore, it is very likely that the NOE observed from the ground to about 0.5 km was due to advection transport of daytime PPO from the southwest sector rather than SST impacts.

3.7 Diagnosis based on measurements of pollutants in the surface layer

To further understand the source characteristic of NOE, the hourly average concentrations of surface PAN (~~peroxyacetic nitric anhydride~~) and O₃ observed at the ZB supersite are displayed in Figure 2. It can be seen that the variations of PAN and O₃ were in phase and the concentrations of both gases were well correlated ($r^2=0.60$, $p<0.0001$, $n=283$), indicating that the variations of PAN and O₃ were driven mainly by chemical and physical processes within the boundary layer. The maximum O₃ from 02:00 LT to 05:00 LT on 1 August was 88 ± 5 ppbv, matching with PAN of 0.44 ± 0.02 ppbv, which was still significantly higher than those lowest values in nighttime of other dates ~~and did not show sign of significant impact of STT~~. As a secondary photochemical pollutant, PAN is thermally unstable but can be transported over higher altitudes, where it has much longer lifetime due to low temperatures. However, observations over the years on mountain tops, aircrafts and satellites showed that the mixing ratios of PAN in the free troposphere and lower stratosphere of the Northern Hemisphere were normally much lower than 0.5 ppb and mostly lower than 0.3 ppb (Singh et al., 2007; Moore and Remedios, 2010; Roiger et al., 2011; Pandey Deolal et al., 2013; Fadnavis et al., 2014; Kramer et al., 2015). PAN decomposes rapidly in warm urban air. According to Cox and Roffey (1977), the lifetime of PAN was only 2.7 hours at 25 °C. In our case, the nighttime temperature at the ZB supersite varied from 33.1 °C at 18:00 LT on 31 July to 20.4 °C at 06:00 LT on 1 August, 2021, with an average of 26.0 °C. Under such warm condition, the thermal decomposition lifetimes were in the range of 0.2-1.3 hours based on the hourly observations. If the surface layer had been significantly impacted by air masses from the free troposphere and lower stratosphere, we would have seen much lower levels of PAN during the NOE instead of the observed 0.4-0.5 ppb (Figure 2). Therefore, given the relative lower concentrations of PAN in the free troposphere and lower stratosphere and the rapid thermal decomposition, it is unlikely that over 0.4 ppb of PAN could be observed in surface air

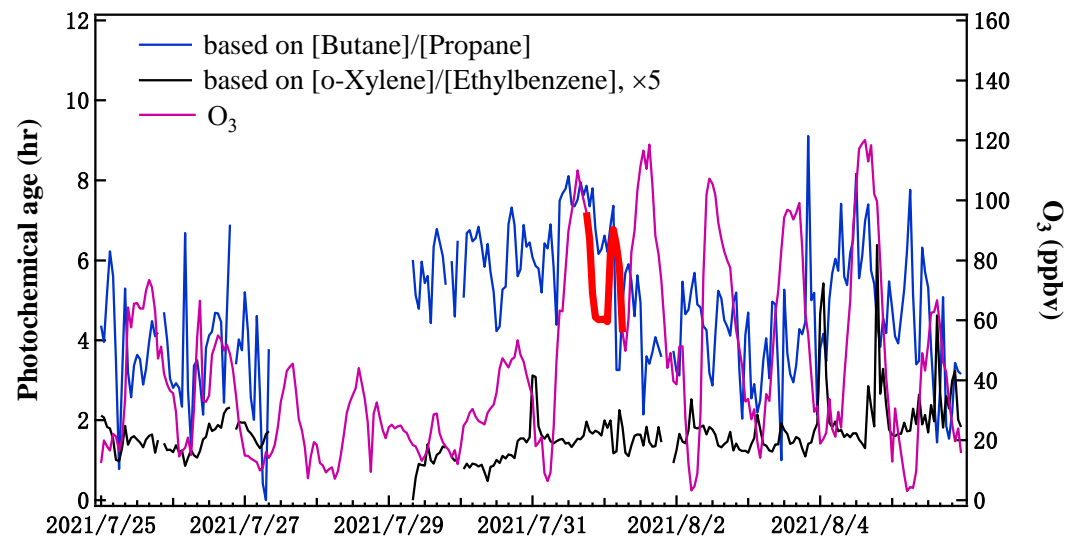
significantly impacted by stratospheric intrusion, not to mention that the PAN values during the NOE were even much higher than the nighttime values before and after the NOE event.



225 **Figure 2. Time series of hourly average of O₃ (purple) and PAN (blue) at the ZB supersite between 25 July and 5 August 2021.**
Data from 18:00 LT on 31 July to 06:00 LT on 1 August are highlighted in red.

Photochemical ages of air masses arrivedarriving at the ZB supersite from 25 July to 5 August 2021 were estimated based on hourly VOCs (volatile organic compounds) measurements. The methodologies of the estimation are given in detail in Text [S1S2](#). Figure 3 shows two sets of estimated photochemical ages based on ratios [Butane]/[Propane] and [o-Xylene]/[Ethylbenzene], respectively, together with hourly O₃ concentrations from the supersite. As can be seen in the figure, photochemical ages estimated based on [o-Xylene]/[Ethylbenzene] are much shorter than those based on [Butane]/[Propane]. Since we used the observed maximum [Butane]/[Propane] and [o-Xylene]/[Ethylbenzene] in the calculations instead of the respective initial [Butane]/[Propane] and [o-Xylene]/[Ethylbenzene], the photochemical ages were underestimated, particularly those based on measurements of o-xylene and ethylbenzene, which are much more reactive than the alkanes (see Text [S1S2](#)). The estimated photochemical ages can be used to check the major conclusion in Chen et al. (2022) even though they could be underestimated. Here, the actual values of photochemical ages are less important than their variations during, before and after the NOE. The photochemical ages of stratospheric air masses are usually longer than one year (Diallo et al., 2012). However, all estimated photochemical ages in Figure 3, including those for the NOE period, are much shorter than one day. More importantly, the photochemical ages for the NOE from 31 July to 1 August 2021 varied roughly in the middle of all estimated ages and showed no drastic increases, which would be expected if the surface air had contained a significant fraction of stratospheric air. Therefore, our observation-based calculations of photochemical ages do not support the

conclusion made by Chen et al. (2022) about the mechanisms of the NOE. It is very likely that the NOE was not a result of typhoon-induced stratospheric intrusion, instead, it was originated from fresh photochemical production of O_3 in the lower troposphere.



245

Figure 3. Variations of estimated photochemical ages of air masses arriving at the ZB supersite and the O_3 mixing ratio (purple). The O_3 data from 18:00 LT on 31 July to 06:00 LT on 1 August 2021 are highlighted in bold red line. The photochemical ages were estimated on the basis of [Butane]/[Propane] (blue) and [o-Xylene]/[Ethylbenzene] (black), respectively.

4 Discussion and Conclusions

250 The NOE event presented by Chen et al. (2022) was actually one of the normal cases of NOE associated with the compensatory downdrafts induced by convection cells (Betts et al., 2002). Occurrences of NOE had been reported in the NCP during the summer (e.g., Ma et al., 2013; Jia et al., 2015). Similar phenomena were found in southern China (He et al., 2021), in the Bay of Bengal in India (Sahu and Lal, 2006) and even in Amazonia (Betts et al., 2002). The daytime PPO is transported upward to and resides in the residual layer, while surface O_3 is largely removed at night mainly by NO_x titrations, 255 forming a large positive lower tropospheric gradient of O_3 from surface to the residual layer during the night and early morning period, as often reported in the literature (e.g., Ma et al., 2013; Jia et al., 2015; Wang et al., 2017; Tang et al., 2017; Zhao et al., 2019; Zhu et al., 2020). The positive gradient of O_3 can be strongly disturbed by nighttime convective processes or low-level jets and the compensatory downdrafts in convection systems can cause NOE events, as reported for a Amazonia site (Betts et al., 2002) and a NCP site (Jia et al., 2015) and systematically summarized in He et al. (2022).

260 Previous investigations on surface O_3 enhancement associated with passage of typhoons revealed two possible mechanisms: i) stratospheric O_3 is ultimately transported to the surface level after typhoon-induced STT (Jiang et al., 2015; Wang et al., 2020; Zhan et al., 2020; Chen et al., 2022; Meng et al., 2022); ii) formation and accumulation of O_3 as well as

emissions of O₃ precursors in the boundary layer are promoted under meteorological conditions accompanying strong atmospheric subsidence in typhoon periphery (Hung and Lo, 2015; Shao et al., 2022; Wang et al., 2022). Directly before the 265 NOE event reported by Chen et al. (2022), the photochemical formation of O₃ in the NCP was obviously intensified after a few days of weakening (Figure 1). The O₃-rich air spread within the boundary layer during the daytime of 31 July and remained in the residual layer at night. Given the favorable thermal-dynamical condition like MCSs, the PPO in the residual layer could easily be conveyed downward to the surface, leading to NOE in the surface layer, as also shown in other studies 270 (Shu et al., 2016; Qu et al., 2021; Ouyang et al., 2022; He et al., 2022). Our analysis supports the conclusion that this NOE event was caused by rapid downward transport of daytime PPO residing in the residual layer.

The STT of O₃ is often observed in the free troposphere through balloon or aircraft-based observations and air masses associated with identified STT of O₃ exhibit usually the feature of HOLWCO. However, air mass with HOLWCO feature in free troposphere do not necessarily mean that the O₃ enhancement is originated from the stratosphere (Stoller et al., 1999). For those observations made at a high mountain site (Izaña, 28°18'N, 16°30'W, 2370 m a.s.l), even with stratospheric tracers 275 (such as ⁷Be), the contribution of PPO to the rise of O₃ at surface level was important and the stratosphere seemed not to be a direct source (Prospero et al., 1995; Graustein and Turekian, 1996). Although the air with HOLWCO, induced by katabatic winds, was observed at the base camp of Mount Everest (about 5000 m a.s.l.), the source of O₃ from the stratosphere was not confirmed (Zhu et al., 2006). Simultaneous observations of O₃ and PAN at the Namco (4545 m a.s.l.) in Tibet captured air masses with high O₃ and low water vapor, which were accompanied with increases of PAN, suggesting that PPO during the 280 long-range transport might be one of the major sources of elevated O₃ (Xu et al., 2018). These examples show that even at high altitude sites, HOLWCO phenomena may not be caused by STT.

In the NOE cases reported in Chen et al. (2022), the HOLWCO feature during the NOE was very much far from the stratospheric characteristics. The maximum O₃ levels were around 80 ppb and significantly lower than respective daytime maxima; the CO levels were between 200 and 500 ppb (see Figure 3 in Chen et al., 2022 and Figure S6), much higher than the CO levels in the middle and upper troposphere (about 100 ppb) and lower stratosphere (<50 ppb) (Inness et al., 2022) and even not lower than those CO values on some other days; the measured water vapor pressure during the NOE was close to its normal values (Figure S6) and did not show any sign of substantial stratospheric impact. In other words, although the levels of CO or water vapor were relatively lower during the NOE events, they did not show large deviations from their values within normal boundary layer, nor substantial STT influences. All these, together with our evidence given above, indicate that the NOE reported in Chen et al. (2022) was not caused by typhoon-induced stratospheric intrusion. Therefore, 285 more cautions should be taken when attributing HOLWCO events at low altitude sites to stratospheric impact, whether or not there was an influence from a typhoon or other synoptic system. It is suggested that if possible, each case should be verified 290 by analyzing both physical and chemical processes before making a conclusion.

Data availability. The data used in this study are available upon request to the corresponding author (xiaobin_xu@189.cn).

295 **Author contributions.** XZ and XX designed the research. WY was responsible for the observations at the Zibo supersite. CG and YL validated the data from the supersite. XZ, YS and XX performed the data analysis. XZ and XX prepared the manuscript.

Competing interests. The contact author has declared that none of the authors has any competing interests.

300 **Financial support.** This research has been supported by the National Natural Science Foundation of China (grant no. 41775031) and the Science and Technology Development Fund of the Chinese Academy of Meteorological Sciences (grant nos. 2023KJ013 and 2023KJ014). The observations at the ZB supersite were supported by the National Research Program for Key Issues in Air Pollution Control (No. DQGG202119, DQGG202137).

References

305 Ahrens, C.D., and Henson, R.: Essential of Meteorology: An Invitation to the Atmosphere (8th Edition), Cengage Learning, Boston, USA, 2016.

Baray, J. L., Ancellet, G., Radriambelo, T., and Baldy, S.: Tropical cyclone Marlene and stratosphere-troposphere exchange, J. Geophys. Res., 104, 13 953–13 970, <https://doi.org/10.1029/1999JD900028>, 1999.

Bethan, S., Vaughan, G., Gerbig, C., Volz-Thomas, A., Richer, H., and Tiddeman, D. A.: Chemical air mass differences near 310 fronts, J. Geophys. Res., 103, 13413–13434, <https://doi.org/10.1029/98JD00535>, 1998.

Betts, A. K., Gatti, L. V., Cordova, A. M., Dias, M. A. S., and Fuentes, J. D.: Transport of ozone to the surface by convective downdrafts at night, J. Geophys. Res.-Atmos., 107, D20, <https://doi.org/10.1029/2000JD000158>, 2002.

Bolton, D.: The computation of equivalent potential temperature, Mon. Weather Rev., 108, 1046-1053, [https://doi.org/10.1175/1520-0493\(1980\)108<1046:TCOEPT>2.0.CO;2](https://doi.org/10.1175/1520-0493(1980)108<1046:TCOEPT>2.0.CO;2), 1980.

315 Cairo, F., Buontempo, C., MacKenzie, A.R., Schiller, C., Volk, C.M., Adriani, A., Mitev, V., Matthey, R., Di Donfrancesco, C., Oulanovshy, A., Ravegnani, F., Yushkov, V., Snels, M., Cagnazzo, C., and Stefanutti, L.: Morphology of the tropopause layer and lower stratosphere above a tropical cyclone: a case study on cyclone Davina (1999), Atmos. Chem. Phys., 8, 3411–3426, <https://doi.org/10.5194/acp-8-3411-2008>, 2008.

Carsey, T. P., and Willoughby, H. E: Ozone measurements from eyewall transects of two Atlantic tropical cyclones, Mon. Weather Rev., 133, 166–174, <https://doi.org/10.1175/MWR-2844.1>, 2005.

320 Chen, J., Peng, Y., Zhang, C., Sun, X., He, X., Liu, C. Mu, Y.: Study and application in calibration method of photochemical synthesis for peroxyacetyl nitrate analyzer (in Chinese with English abstract), Environmental Chemistry, 40(6): 1862–1870, doi: 10.7524/j.issn.0254-6108.2020012003 , 2021.

Chen, Z., Liu, J., Cheng, X., Yang, M., and Wang, H.: Positive and negative influences of typhoons on tropospheric ozone
325 over southern China, *Atmos. Chem. Phys.*, 21, 16911–16923, <https://doi.org/10.5194/acp-21-16911-2021>, 2021.

Chen, Z., Liu, J., Qie, X., Cheng, X., Shen, Y., Yang, M., Jiang, R., and Liu, X.: Transport of substantial stratospheric ozone
to the surface by a dying typhoon and shallow convection, *Atmos. Chem. Phys.*, 22, 8221–8240,
https://doi.org/10.5194/acp-22-8221-2022, 2022.

330 Cho, J.Y.N., Newell, R.E., Browell, E.V., Grant, W.B., Butler, C.F., and Fenn, M.A.: Observation of pollution plume
capping by a tropopause fold, *Geophys. Res. Lett.*, 28(17), 3243–3246, <https://doi.org/10.1029/2001GL012898>, 2001.

Cooper, O. R., Moody, J. L., Parrish, D. D., Trainer, M., Holloway, J. S., Hubler, G., Fehsenfeld, F. C., and Stohl, A.: Trace
gas composition of midlatitude cyclones over the western North Atlantic Ocean: A seasonal comparison of O₃ and CO, *J. Geophys. Res.*, 107, D7, <https://doi.org/10.1029/2001JD000902>, 2002.

335 Cox, R.A. and Roffey, M.J.: Thermal decomposition of peroxyacetyl nitrate in the presence of nitric oxide, *Environ. Sci. Technol.*, 11, 900–906, 1977.

Diallo, M., Legras, B., and Che ñin, A.: Age of stratospheric air in the ERA-Interim, *Atmos. Chem. Phys.*, 12, 12133–12154,
doi:10.5194/acp-12-12133-201, 2012.

de Bellevue, J.L., Baray, J.L., Baldy, S., Ancellet, G., Diab, R., Ravetta, F.: Simulations of stratospheric to tropospheric
transport during the tropical cyclone Marlene event. *Atmos. Environ.* 41, 6510–6526,
340 <https://doi.org/10.1016/j.atmosenv.2007.04.040>, 2007.

Ding, A.J., Wang, T., Thouret, V., Cammas, J.-P., and N éd éc, P.: Tropospheric ozone climatology over Beijing: analysis of
aircraft data from the MOZAIC program, *Atmos. Chem. Phys.*, 8, 1–13, <https://doi.org/10.5194/acp-8-1-2008>, 2008.

345 Fadnavis, S., Schultz, M.G., Semeniuk, K., Mahajan, A.S., Pozzoli, L., Sonbawne, S., Ghude, S.D., Kiefer, M., and Eckert,
E.: Trends in peroxyacetyl nitrate (PAN) in the upper troposphere and lower stratosphere over southern Asia during the
summer monsoon season: regional impacts, *Atmos. Chem. Phys.*, 14, 12725–12743, <https://doi.org/10.5194/acp-14-12725-2014>, 2014.

Graustein, W.C., and Turekian, K.K.: ⁷Be and ²¹⁰Pb indicate upper troposphere source for elevated ozone in the summertime
subtropical free troposphere of the eastern North Atlantic, *Geophys. Res. Lett.*, 23, 5, 539–542,
<https://doi.org/10.1029/96GL00304>, 1996.

350 He, C., Lu, X., Wang, H., Wang, H., Li, Y., He, G., He, Y., Wang, Y., Zhang, Y., Liu, Y., Fan, Q., and Fan, S.: The
unexpected high frequency of nocturnal surface ozone enhancement events over China: characteristics and mechanisms,
Atmos. Chem. Phys., 22, 15243–15261, <https://doi.org/10.5194/acp-22-15243-2022>, 2022.

He, Y., Wang, H., Wang, H., Xu, Y., Li, Y., Fan, S.: Meteorology and topographic influences on nocturnal ozone increase
during the summertime over Shaoguan, China, *Atmospheric Environment*, 256, 118459,
355 <https://doi.org/10.1016/j.atmosenv.2021.118459>, 2021.

Hung, C.-H. and Lo, K.-C.: Relationship between ambient ozone concentration changes in southwestern Taiwan and
invasion tracks of tropical typhoons, *Adv. Meteorol.*, 2015, 402976, <https://doi.org/10.1155/2015/402976>, 2015.

Holton, J. R., Haynes, P. H., McIntyre, M. E., Douglass, A. R., Rood, R. B., and Pfister, L.: Stratosphere-troposphere exchange, *Rev. Geophys.*, 33, 403-439, <https://doi.org/10.1029/95RG02097>, 1995.

360 Inness, A., Aben, I., Ades, M., Borsdorff, T., Flemming, J., Jones, L., Landgraf, J., Langerock, B., Nedelec, P., Parrington, M., and Ribas, R.: Assimilation of S5P/TROPOMI carbon monoxide data with the global CAMS near-real-time system, *Atmos. Chem. Phys.*, 22, 14355–14376, <https://doi.org/10.5194/acp-22-14355-2022>, 2022.

Jaeglé, L., Jacob, D. J., Brune, W. H., Tan, D., Faloona, I. C., Weinheimer, A. J., and Ridley, B.A., Campos, T.L., Sachse, G.W.: Sources of HO_x and production of ozone in the upper troposphere over the United States, *Geophysical Research Letters*, 25, 1709–1712, <https://doi.org/10.1029/98GL0004>, 1998.

365 Jia, S., Xu, X., Lin, W., Wang, Y., He, X., and Hualong, Z.: Increased Mixing Ratio of Surface Ozone by Nighttime Convection Process over the North China Plain (in Chinese with English abstract), *J. Appl. Meteor. Sci.*, 26, 280–290, <https://doi.org/10.11898/1001-7313.20150303>, 2015.

Jiang, Y. C., Zhao, T. L., Liu, J., Xu, X. D., Tan, C. H., Cheng, X. H., Bi, X. Y., Gan, J. B., You, J. F., and Zhao, S. Z.: Why 370 does surface ozone peak before a typhoon landing in southeast China?, *Atmos. Chem. Phys.*, 15, 13331–13338, <https://doi.org/10.5194/acp-15-13331-2015>, 2015.

Kramer, L.J., Helming, D., Burkhardt, J.F., Stohl, A., Oltmans, S., and Honrath, R.E.: Seasonal variability of atmospheric nitrogen oxides and non-methane hydrocarbons at the GEOSummit station, Greenland, *Atmos. Chem. Phys.*, 15, 6827–6849, <https://doi.org/10.5194/acp-15-6827-2015>, 2015.

375 Lelieveld, J., and Dentener, F. J.: What controls tropospheric ozone?, *J. Geophys. Res.*, 105(D3), 3531–3551. <https://doi.org/10.1029/1999JD901011>, 2000.

Logan, J. A.: Tropospheric ozone: Seasonal behavior, trends, and anthropogenic influence, *J. Geophys. Res.*, 90(D6), 10,463–10,482, <https://doi.org/10.1029/JD090iD06p10463>, 1985.

380 Lu, X., Hong, J., Zhang, L., Cooper, O.R., Schultz, M.G., Xu, X., Wang, T., Gao, M., Zhao, Y., Zhang, Y.: Severe Surface Ozone Pollution in China: A Global Perspective, *Environ. Sci. Technol. Lett.*, 2018, 5 (8), 487–494, DOI: 10.1021/acs.estlett.8b00366, 2018.

Lyu, X., Li, K., Guo, H., Morawska, L., Zhou, B., Zeren, Y., Jiang, F., Chen, C., Goldstein, A., Lin, M., Xu, X., Wang, T., Lu, X., Zhu, T., Querol, X., Chatani, S., Latif, M.T., Schuch, D., Sinha, V., Kumar, P., Mullins, B., Seguel, R., Shao, M., Xue, L., Wang, N., Chen, J., Gao, J., Chai, F., Simpson, I., Sinha, B., Blake, D.: A synergistic ozone-climate control to 385 address emerging ozone pollution challenges, *One Earth*, 6, 964-977, <https://doi.org/10.1016/j.oneear.2023.07.004>, 2023.

Ma, Z.Q., Xu, H.H., Meng, W., Zhang, X.L., Xu, J., Liu, Q., Wang, Y.S.: Vertical ozone characteristics in urban boundary layer in Beijing, *Environ. Monit. Assess.*, 185, 5449–5460. <https://doi.org/10.1007/s10661-012-2958-5>, 2013.

Ma, Z., Xu, J., Quan, W., Zhang, Z., Lin, W., and Xu, X.: Significant increase of surface ozone at a rural site, north of 390 eastern China, *Atmos. Chem. Phys.*, 16, 3969-3977, doi:10.5194/acp-16-3969-2016, 2016.

390 Meng, K., Zhao, T., Xu, X., Hu, Y., Zhao, Y., Zhang, L., Pang, Y., Ma, X., Bai, Y., Zhao, Y., Zhen, S.: Anomalous surface O₃ changes in North China Plain during the northwestward movement of a landing typhoon, *Sci. Total Environ.*, 820, 153196, <https://doi.org/10.1016/j.scitotenv.2022.153196>, 2022.

Merrill, R. T.: Characteristics of the Upper-tropospheric Environmental flow around Hurricanes, *J. Atmos. Sci.*, 45, 1665–1677, [https://doi.org/10.1175/1520-0469\(1988\)045<1665:COTUTE>2.0.CO;2](https://doi.org/10.1175/1520-0469(1988)045<1665:COTUTE>2.0.CO;2), 1988.

395 | **Moore, D. P. and Remedios, J. J.: Seasonality of Peroxyacetyl nitrate (PAN) in the upper troposphere and lower stratosphere using the MIPAS-E instrument, *Atmos. Chem. Phys.*, 10, 6117–6128, <https://doi.org/10.5194/acp-10-6117-2010>, 2010.**

Newell, R.E., Hu, W., Wu, Z.-X., Zhu, Y., Akimoto, H., Anderson, B.E., Browell, E.V., Gregory, G.L., Sachse, G.W., Shippert, M.C., Bachmeier, A.S., Bandy, A.R., Thornton, D.C., Blake, D.R., Rowland, F.S., Bradshaw, J.D., Crawford, J.H., Davis, D.D., Sandholm, S.T., Brockett, W., DeGreef, L., Lewis, D., McCormick, D., Monitz, E., Collins, J.E., Heikes, B.G., Merrill, J.T., Kelly, K.K., Liu, S.C., Kondo, Y., Koike, M., Liu, C.-M., Sakamaki, F., Singh, H.B., Dibb, J.E., and Talbot, R.W.: Atmospheric sampling of Super typhoon Mireille with NASA DC-8 aircraft on September 27, 1991, during PEM-West A, *J. Geophys. Res.*, 101, 1853–1871, <https://doi.org/10.1029/95JD01374>, 1996a.

400 | Newell, R.E., Wu, Z.-X., Zhu, Y., Hu, W., Browell, E.V., Gregory, G.L., Sachse, G.W., Collins Jr., J.E., Kelly, K.K., and Li, S.C.: Vertical fine-scale atmospheric structure measured from NASA DC-8 during PEM-West A, *J. Geophys. Res.*, 101(D1), 1,943–1,960, <https://doi.org/10.1029/95JD02613>, 1996b.

405 | **Ouyang, S., Deng, T., Liu, R., Chen, J., He, G., Leung, J. C.-H., Wang, N., and Liu, S. C.: Impact of a subtropical high and a typhoon on a severe ozone pollution episode in the Pearl River Delta, China, *Atmos. Chem. Phys.*, 22, 10751–10767, <https://doi.org/10.5194/acp-22-10751-2022>, 2022.**

410 | **Pandey Deolal, S., Staehelin, J., Brunner, D., Cui, J., Steinbacher, M., Zellweger, C., Henne, S., and Vollmer, M.K.: Transport of PAN and NO_x from different source regions to the Swiss high alpine site Jungfraujoch, *Atmos. Environ.*, 64, 103–115, <https://doi.org/10.1016/j.atmosenv.2012.08.021>, 2013.**

Parrish, D.D., Trainer, M., Holloway, J.S., Yee, J.E., Warshawsky, M.S., Fehsenfeld, F.C., Forbes, G.L., and Moody, J.L.: Relationships between ozone and carbon monoxide at surface sites in the North Atlantic region, *J. Geophys. Res.*, 103, 13,357–13,376, <https://doi.org/10.1029/98JD00376>, 1998.

415 | Preston, A., Fuelberg, H., and Barth, M.: Simulation of chemical transport by Typhoon Mireille, *J. Geophys. Res.: Atmospheres*, 124, 11,614–11,639, <https://doi.org/10.1029/2019JD030446>, 2019.

Prospero, J.M., Schmitt, R., Cuevas, E., Savoie, D.L., Graustein, W.C., Turekian, K.K., Volz-Thomas, A., Diaz, A., Oltmans, S.J., and Levy II, H.: Temporal variability of summer-time ozone and aerosols in the free troposphere over the eastern North Atlantic, *Geophys. Res. Lett.*, 22, 2925–2928, <https://doi.org/10.1029/95GL02791>, 1995.

420 | Qu, K., Wang, X., Yan, Y., Shen, J., Xiao, T., Dong, H., Zeng, L., and Zhang, Y.: A comparative study to reveal the influence of typhoons on the transport, production and accumulation of O₃ in the Pearl River Delta, China, *Atmos. Chem. Phys.*, 21, 11593–11612, <https://doi.org/10.5194/acp-21-11593-2021>, 2021.

425 Ouyang, S., Deng, T., Liu, R., Chen, J., He, G., Leung, J. C. H., Wang, N., and Liu, S. C.: Impact of a subtropical high and a typhoon on a severe ozone pollution episode in the Pearl River Delta, China, *Atmos. Chem. Phys.*, 22, 10751–10767, <https://doi.org/10.5194/acp-22-10751-2022, 2022>.

Roiger, A., Aufmhoff, H., Stock, P., Arnold, F., and Schlager, H.: An aircraft-borne chemical ionization – ion trap mass spectrometer (CI-ITMS) for fast PAN and PPN measurements, *Atmos. Meas. Tech.*, 4, 173–188, <https://doi.org/10.5194/amt-4-173-2011, 2011>.

430 Roux, F., Clark, H., Wang, K.-Y., Rohs, S., Sauvage, B., and Néeldec, P.: The influence of typhoons on atmospheric composition deduced from IAGOS measurements over Taipei, *Atmos. Chem. Phys.*, 20, 3945–3963, <https://doi.org/10.5194/acp20-3945-2020, 2020>.

Sahu, L.K., and Lal, S.: Changes in surface ozone levels due to convective downdrafts over the Bay of Bengal, *Geophys. Res. Lett.*, 33, L10807, doi:10.1029/2006GL025994, 2006.

435 Shao, M., Yang, J., Wang, J., Chen, P., Liu, B., and Dai, Q.: Co-occurrence of surface O₃, PM_{2.5} pollution, and tropical cyclones in China, *J. Geophys. Res.: Atmospheres*, 127, e2021JD036310, <https://doi.org/10.1029/2021JD036310, 2022>.

Shu, L., Xie, M., Wang, T., Gao, D., Chen, P., Han, Y., Li, S., Zhuang, B., and Li, M.: Integrated studies of a regional ozone pollution synthetically affected by subtropical high and typhoon system in the Yangtze River Delta region, China, *Atmos. Chem. Phys.*, 16, 15801–15819, <https://doi.org/10.5194/acp-16-15801-2016, 2016>.

440 Singh, H.B., Salas, L., Herlth, D., Kolyer, R., Czech, E., Avery, M., Crawford, J.H., Pierce, R.B., Sachse, G.W., Blake, D.R., Cohen, R.C., Bertram, T.H., Perring, A., Wooldridge, P.J., Dibb, J., Huey, G., Hudman, R.C., Turquety, S., Emmons, L.K., Flocke, F., Tang, Y., Carmichael, G.R., and Horowitz, L.W.: Reactive nitrogen distribution and partitioning in the North American troposphere and lowermost stratosphere, *J. Geophys. Res.*, 112, D12S04, <https://doi.org/10.1029/2006JD007664, 2007>.

Škerlak, B., Sprenger, M., and Wernli, H.: A global climatology of stratosphere–troposphere exchange using the ERA-445 Interim data set from 1979 to 2011, *Atmos. Chem. Phys.*, 14, 913–937, doi:10.5194/acp-14-913-2014, 2014.

Stoller, P., Cho, J.Y.N., Newell, R.E., Thouret, V., Zhu, Y., Carroll, M.A., Albercook, G.M., Anderson, B.E., Barrick, J.D.W., Browell, E.V., Gregory, G.L., Sachse, G.W., Vay, S., Bradshaw, J.D., and Sandholm, S.: Measurements of atmospheric layers from the NASA DC-8 and P-3B aircraft during PEM-Tropics A, *J. Geophys. Res.: Atmospheres*, 104, D5, 5745–5764, <https://doi.org/10.1029/98JD02717, 1999>.

450 Tang, G., Zhu, X., Xin, J., Hu, B., Song, T., Sun, Y., Zhang, J., Wang, L., Cheng, M., Chao, N., Kong, L., Li, X., and Wang, Y.: Modelling study of boundary-layer ozone over northern China - Part I: Ozone budget in summer, *Atmos. Res.*, 187, 128–137, doi: 10.1016/j.atmosres.2016.10.017, 2017.

Wang, H., Wang, W., Huang, X., and Ding, A.: Impacts of stratosphere-to-troposphere-transport on summertime surface ozone over eastern China, *Sci. Bull.*, 65, 276–279, <https://doi.org/10.1016/j.scib.2019.11.017, 2020>.

455 Wang, R., Xu, X., Jia, S., Ma, R., Ran, L., Deng, Z., Lin, W., Wang, Y., and Ma, Z.: Lower tropospheric distributions of O₃ and aerosol over Raoyang, a rural site in the North China Plain, *Atmos. Chem. Phys.*, 17, 3891-3903, doi:10.5194/acp-17-3891-2017, 2017.

Wang, N., Huang, X., Xu, J., Wang, T., Tan, Z., and Ding, A.: Typhoon-boosted biogenic emission aggravates cross-regional ozone pollution in China, *Sci. Adv.*, 8, eabl6166, DOI: 10.1126/sciadv.abl6166, 2022.

460 Xu, X., Zhang, H., Lin, W., Wang, Y., Xu, W., and Jia, S.: First simultaneous measurements of peroxyacetyl nitrate (PAN) and ozone at Nam Co in the central Tibetan Plateau: impacts from the PBL evolution and transport processes, *Atmos. Chem. Phys.*, 18, 5199–5217, <https://doi.org/10.5194/acp-18-5199-2018>, 2018.

Zhan, C., Xie, M., Huang, C., Liu, J., Wang, T., Xu, M., Ma, C., Yu, J., Jiao, Y., Li, M., Li, S., Zhuang, B., Zhao, M., and Nie, D.: Ozone affected by a succession of four landfall typhoons in the Yangtze River Delta, China: major processes and 465 health impacts, *Atmos. Chem. Phys.*, 20, 13781–13799, <https://doi.org/10.5194/acp-20-13781-2020>, 2020.

Zhao, W., Tang, G., Yu, H., Yang, Y., Wang, Y., Wang, L., An, J., Gao, W., Hu, B., Cheng, M., An, X., Li, X., and Wang, Y.: Evolution of boundary layer ozone in Shijiazhuang, a suburban site on the North China Plain, *J. Environ. Sci.*, 83, 152-160, doi: 10.1016/j.jes.2019.02.016, 2019.

Zhu, T., Lin, W., Song, Y., Cai, X., Zou, H., Kang, L., Zhou, L., and Akimoto, H.: Downward transport of ozone-rich air 470 near Mt. Everest, *Geophys. Res. Lett.*, 33, L23809, doi:10.1029/2006GL027726, 2006.

Zhu, X., Ma, Z., Qiu, Y., Liu, H., Liu, Q., and Yin, X.: An evaluation of the interaction of morning residual layer ozone and mixing layer ozone in rural areas of the North China Plain, *Atmospheric Research*, 236, 104788, <https://doi.org/10.1016/j.atmosres.2019.104788>, 2020.

Supplement of Comment on “Transport of substantial stratospheric ozone to the surface by a dying typhoon and shallow convection” by Chen et al. (2022)

5 Xiangdong Zheng¹, Wen Yang², Yuting Sun^{1,3}, Chunmei Geng², Yingying Liu², Xiaobin Xu¹

|¹**Key Laboratory for Atmospheric Chemistry of CMA & Institute of the Tibet Plateau**, Chinese Academy of Meteorological Sciences, Beijing 100081, China

²State Key Laboratory of Environmental Criteria and Risk Assessment, Chinese Research Academy of Environmental Sciences, Beijing 100012, China

10 ³Nanjing University of Information Science & Technology, Nanjing, Jiangsu, 210044, China

Correspondence to: Xiaobin Xu (xiaobin_xu@189.cn)

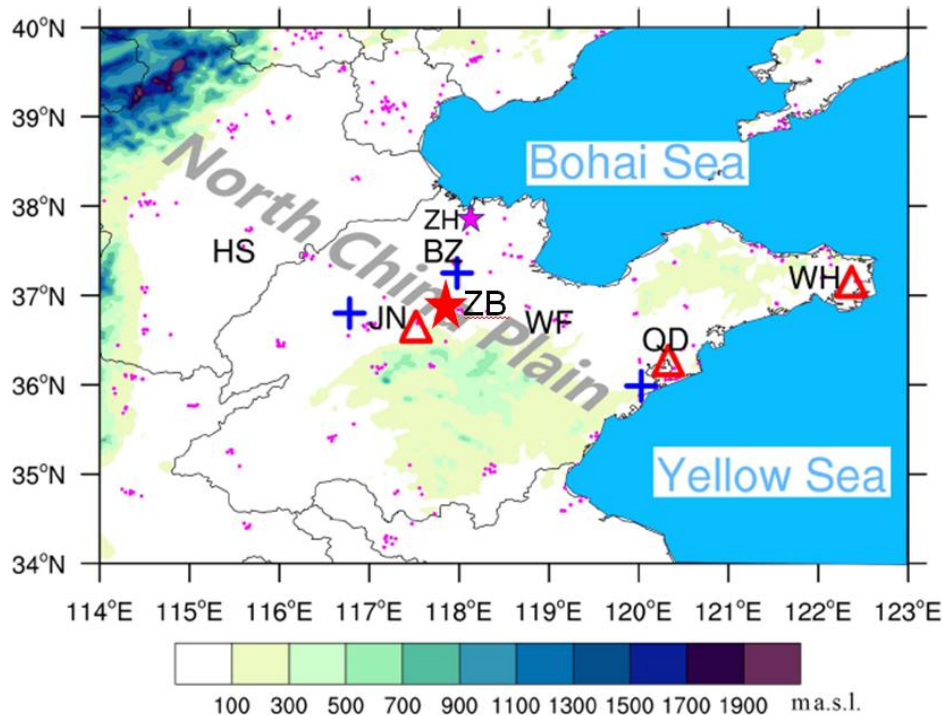


Figure S1: Map modified from Figure 1 in Chen et al. (2022) showing the NCP and its topography with locations of related cities Hengshui (HS), Jinan (JN), Binzhou (BZ), Weifang (WF), Qingdao (QD), Weihai (WH), and Zibo (ZB, red star, newly added in this study). ZB roughly occupies the area of 36.5 °–36.8 °N and 117.9 °–118.0 °E. Other details see Chen et al. (2022).

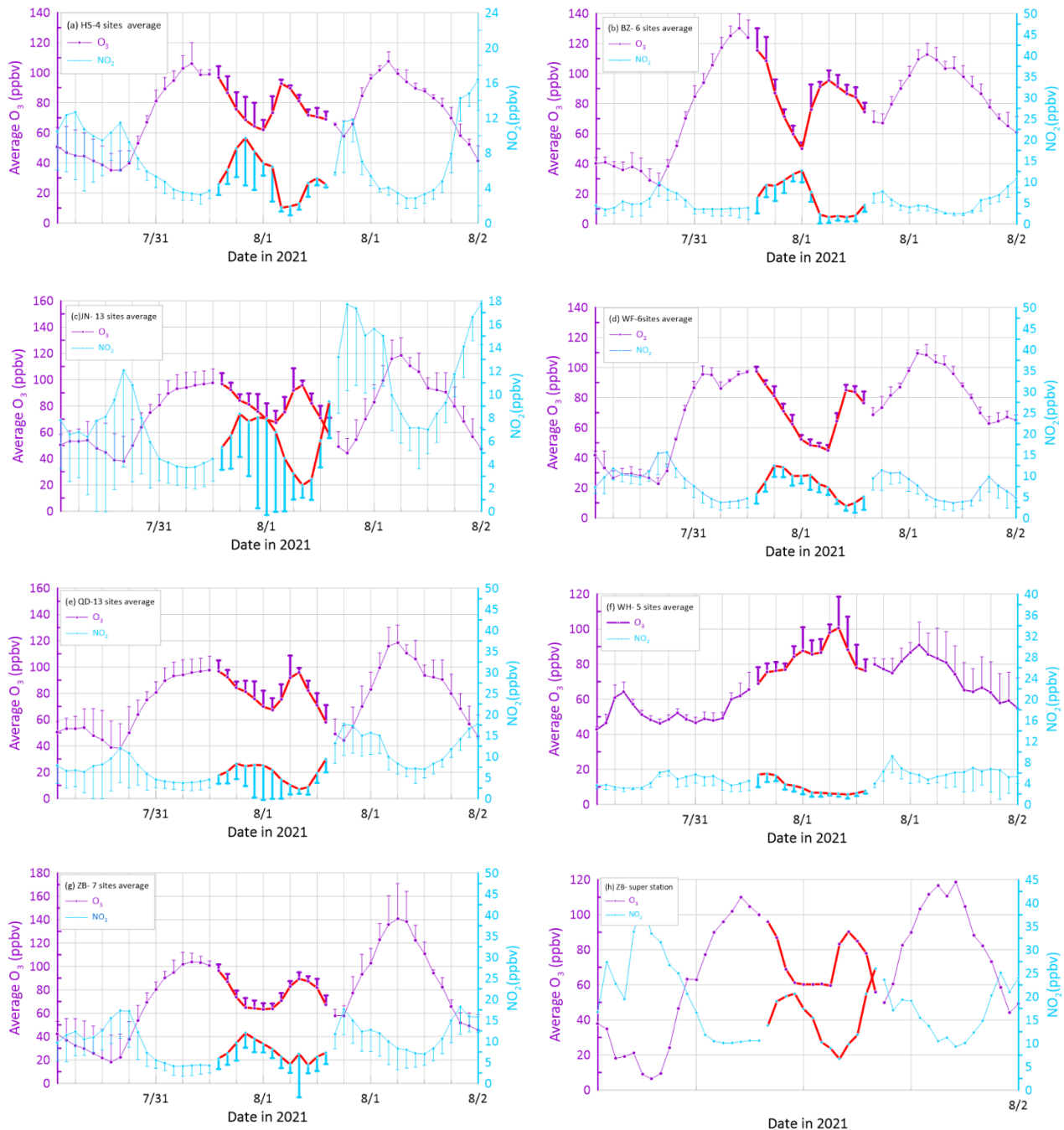


Figure S2. same as Figure 1 but showing only the period from 00:00 LT, 31 July to 23:00 LT, 1 August to highlight the NOEs. The error bars indicate one standard deviations of average O_3 (up) and NO_2 (down).

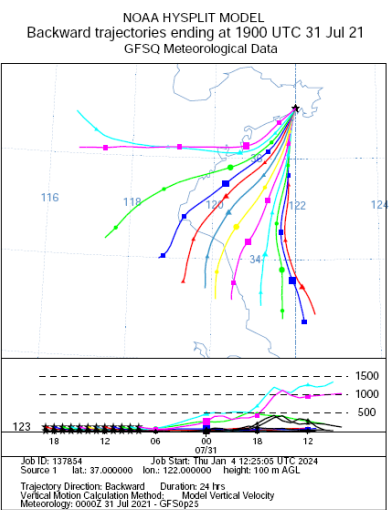
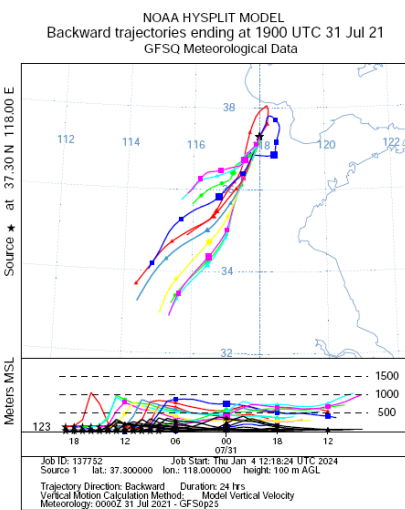
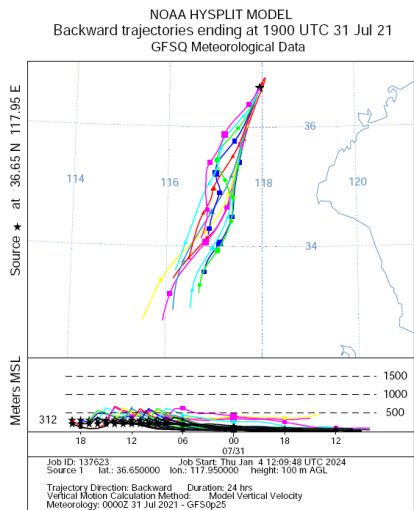


Figure S3. Backward trajectories for air parcels arriving at 100 m above ground over Zibo (ZB, left), Binzhou (BZ, middle) and Weihai (WH, right) every hour between 19:00 and 08:00 UTC, 31 July 2021. The trajectories were computed online using the HYSPLIT model (<https://www.ready.noaa.gov/HYSPLIT.php>; Stein et al. 2015; Rolph et al., 2017) and the Global Forecast System (GFS) reanalysis data (0.25 ° resolution, https://www.emc.ncep.noaa.gov/emc/pages/numerical_forecast_systems/gfs.php). The total run time for the trajectories was 24 hours.

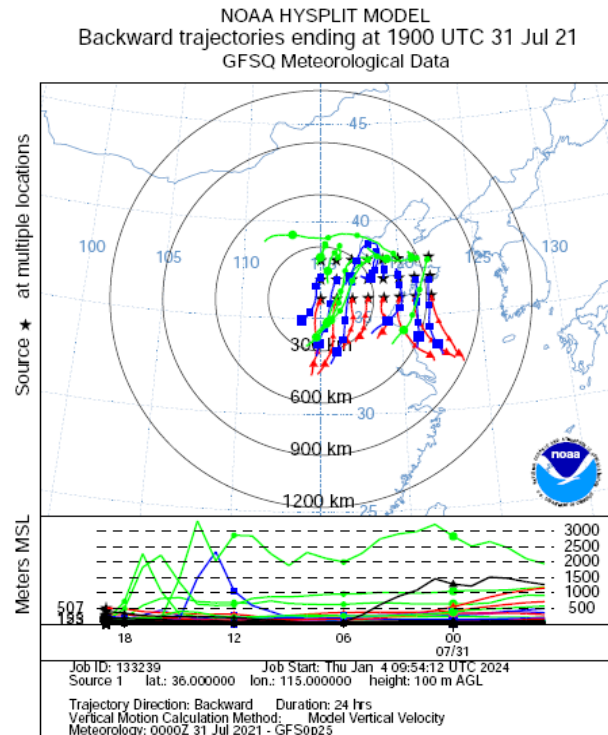


Figure S4. Matrix of backward trajectories for air parcels arriving at 100 m above ground over the domain 36°-38°N and 115°-122°E at 19:00 UTC, 31 July 2021. The trajectories were computed online using the HYSPLIT model (<https://www.ready.noaa.gov/HYSPLIT.php>; Stein et al. 2015; Rolph et al., 2017) and the Global Forecast System (GFS) reanalysis data (0.25 ° resolution, https://www.emc.ncep.noaa.gov/emc/pages/numerical_forecast_systems/gfs.php). The total run time for the trajectories was 24 hours.

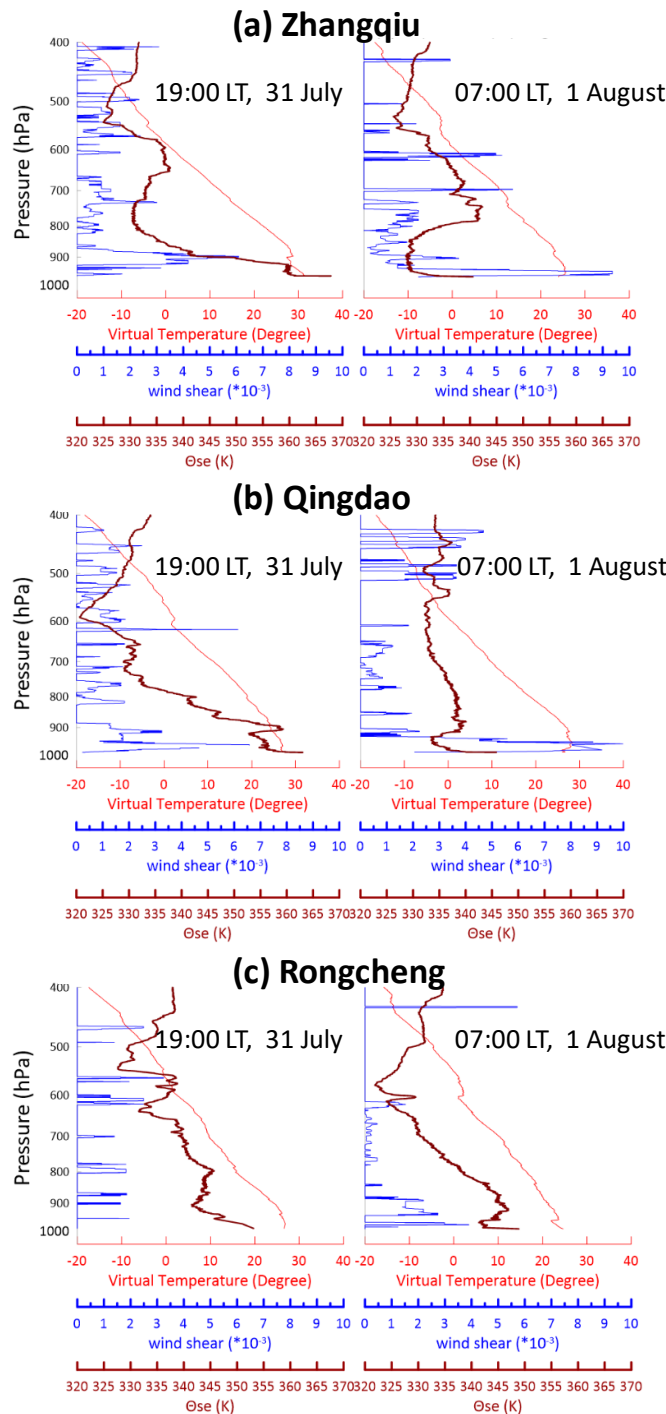


Figure S5. The vertical profiles of virtual temperature (red), equivalent potential temperature (Θ_{se} , grey) and wind shear (blue) calculated on the basis of routine radiosonde observations data at 19:00 LT, 31 July and 07:00 LT, 1 August 2021 in Zhangqiu (ZQ)(a), Qingdao (QD) (b) and Rongcheng (RC) (c).

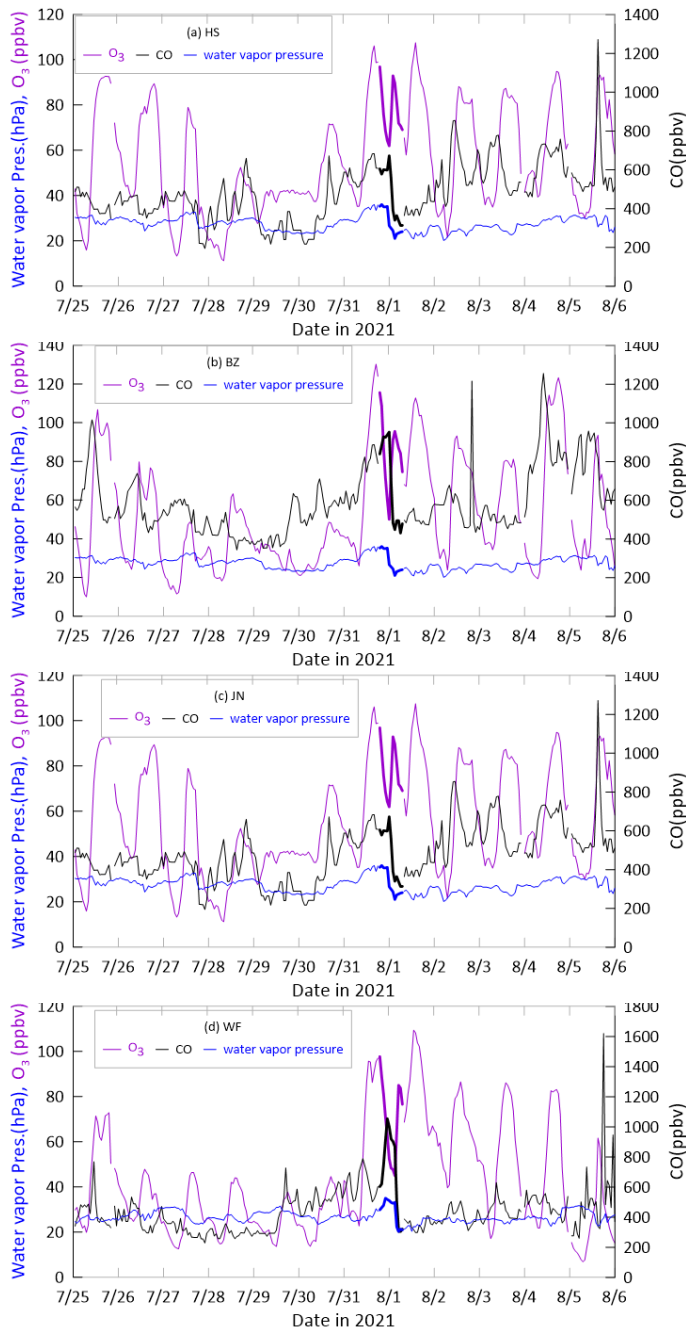


Figure S6. Time series of hourly multi-sites-averages of O_3 (purple), CO (black) and water vapor pressure (blue) between 25 July and 5 August 2021. Data from 18:00 LT on 31 July to 06:00 LT on 1 August are highlighted in thick lines. The multi-site data from HS (4 sites) (a), BZ (6 sites) (b), JN (13 sites) (c), WF (6 sites) (d), QD (13 sites) (e), WH (5 sites) (f) and ZB (7 sites) (g) are available at <https://quotsoft.net/air> (last access: 15 April 2023; X. L. Wang, 2020). Data from the ZB supersite (h) is provided by the Chinese Academy of Environmental Sciences (CRAES). Water vapor pressure data are from <https://data.cma.cn/>.

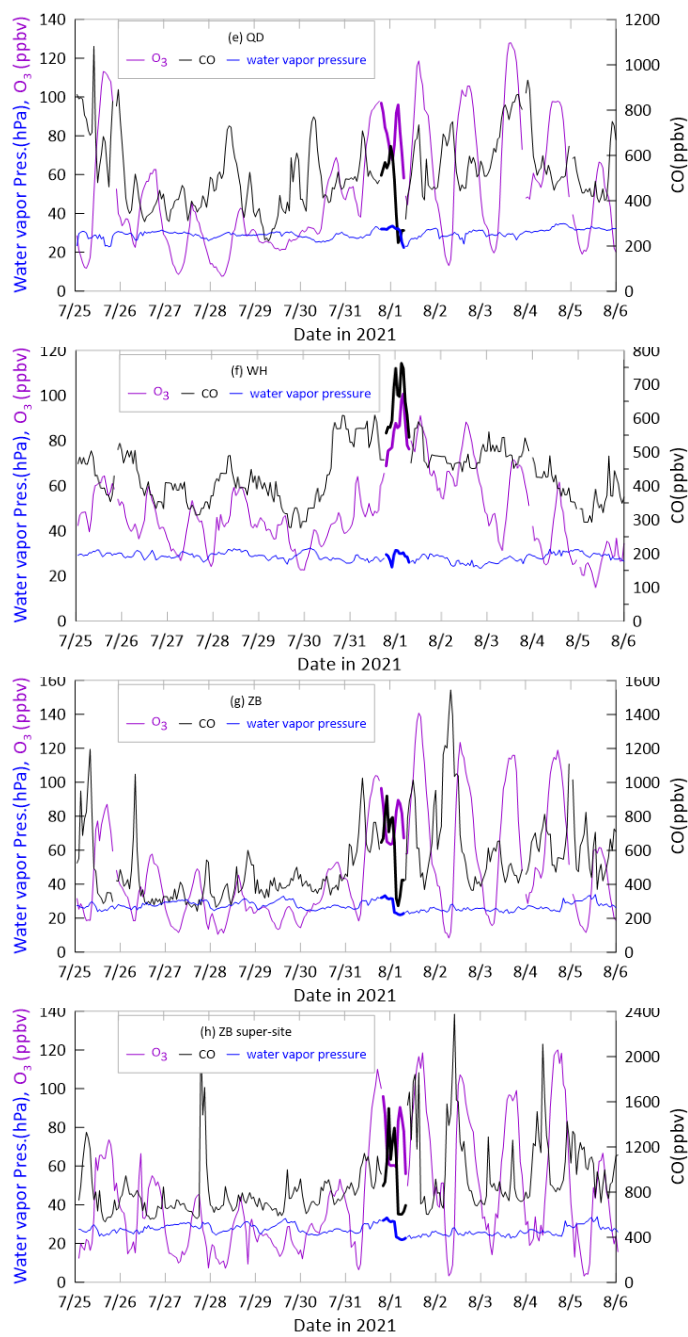


Figure S6. (continued).

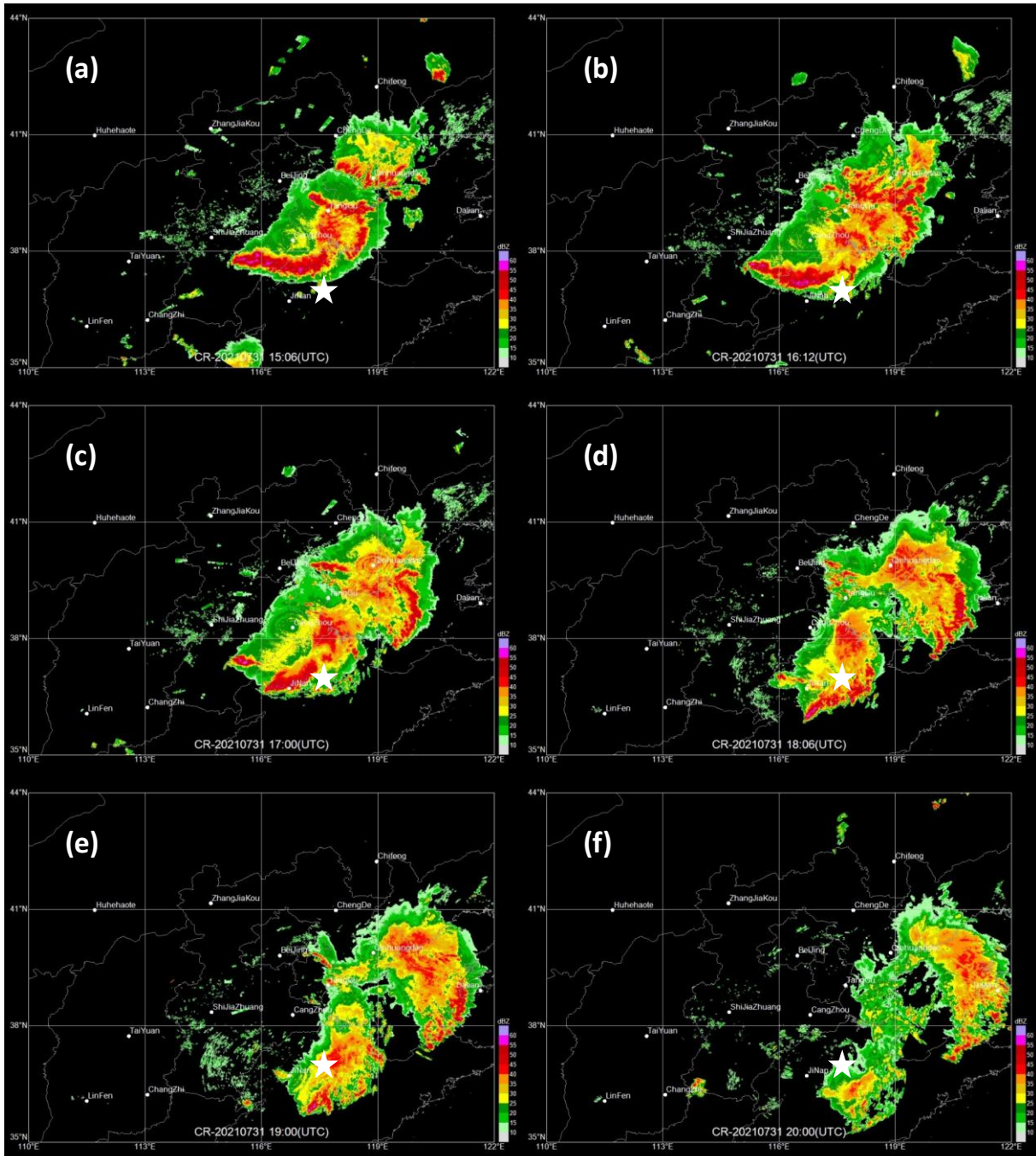


Figure S7. Radar reflectivity maps for the North China Plain at (a) 15:06 UTC (23:00 LT, 31 July), (b) 16:12 UTC (00:12 LT, 1 August), (c) 17:00 UTC (01:00 LT, 1 August), (d) 18:06 UTC (02:06 LT, 1 August), (e) 19:00 UTC (03:00 LT, 1 August) and (f) 20:00 UTC (04:00 LT, 1 August). Some of the major cities are indicated on the maps. The white star on each map shows the location of Zibo. The radar reflectivity maps were provided by Institute of Artificial Intelligence for Meteorology (IAIM), Chinese Academy of Meteorological Sciences (CAMS).

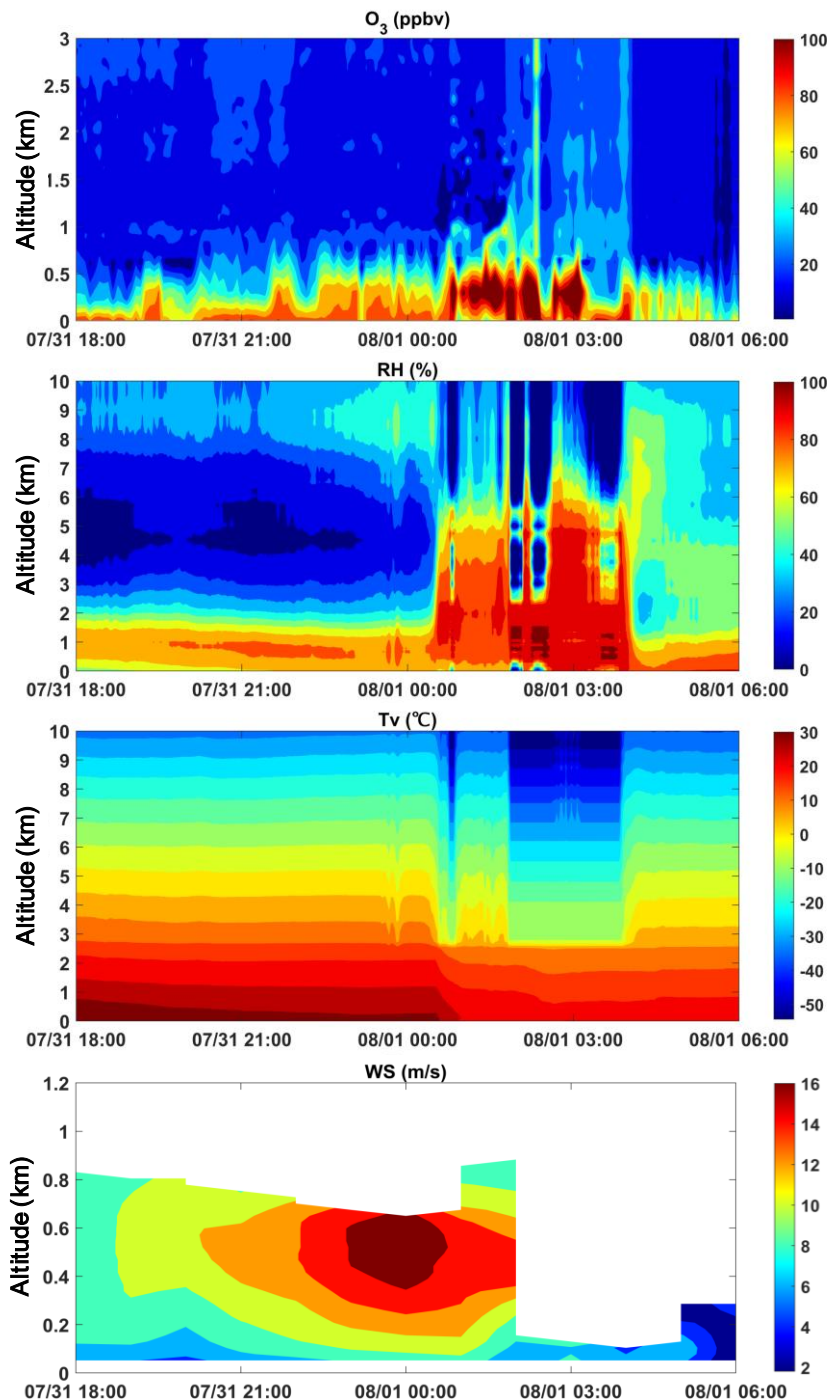


Figure S8. Time-altitude cross sections of O₃, relative humidity (RH), virtual temperature (Tv) and wind speed (WS) observed at the ZB supersite between 18:00 LT, 31 July and 06:00 LT, 1 August 2021. Vertical profiles of O₃ were obtained by a Lidar (RayOL-GB, Anhui Kechuang Zhongguang Technology Co., Ltd., China). Profiles of RH and Tv were detected by a microwave radiometer (KT-001, Qingdao Tianlang Environmental Technology Co., Ltd., China). Vertical distributions of WS were observed by a wind profiler radar (WindPrint V2000, Qingdao Huanhang Safety Environment Technology Co., Ltd, China).

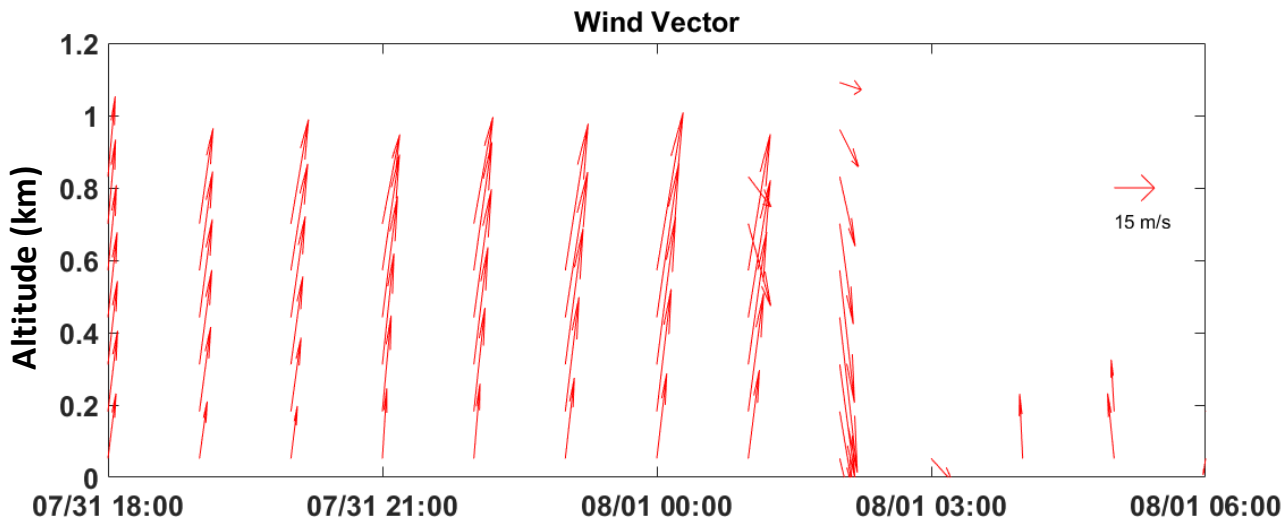


Figure S9. Hourly averaged wind vector below 1 km over the ZB supersite between 18:00 LT, 31 July and 06:00 LT, 1 August 2021. Wind data were observed by a wind profiler radar (WindPrint V2000, Qingdao Huanhang Safety Environment Technology Co., Ltd, China).

Text S1 Identifying potential origin of the NOE by comparing afternoon O₃ with O_x in the NBL during the NOE

Our intention is to check whether or not surface O₃ observed during the NOE contained significant contribution of O₃ from the stratosphere. For this purpose, a comparison of O₃ levels in the vertical direction is helpful. However, O₃ is very reactive and can be significantly removed by titration reactions in the boundary layer, with O₃ + NO = NO₂ + O₂ being the most important one. Therefore, O_x (O₃+NO₂) is a more conserved quantity than O₃ and hence a better metric for comparison (Kley et al., 1994; Kleinmann et al., 2002; Caputi et al., 2019; He et al., 2022). During daytime, NO₂ formed in the titration reaction is rapidly photolyzed to regenerate O₃ so that the net chemical loss of O₃ is relatively small. At night, however, the reaction between O₃ and NO leads to lower levels of O₃ in the nocturnal boundary layer (NBL) and in the residual layer (RL). Because the emission of NO takes place mainly in the NBL, much more O₃ is removed by the titration reaction in the NBL than in the RL (Wang et al., 2018; Caputi et al., 2019; He et al., 2022). In addition, O₃ in the NBL is subjected to dry deposition. Therefore, the O₃ level before sunset largely remains in the RL (Caputi et al., 2019; He et al., 2022) and is usually much higher in the RL than in the NBL under normal conditions.

Following the method of He et al. (2022), we make comparison of afternoon O₃ averages on 31 July with the respective O_x averages in the NBL during the NOE between 31 July and 1 August, 2021. To facilitate the comparison, we treat the average surface O₃ during 14:00-17:00 LT of 31 July as afternoon average of O₃ in the convective boundary layer, denoted as [O₃]_{aft}. Let us now focus on three nighttime atmospheric conditions, (I) undisturbed, (II) disturbed with NOE but no STT impact, and (III) disturbed with NOE and significant STT impact.

Under undisturbed condition (I), the nighttime average O₃ concentration in the RL ([O₃]_{RL}) should be close to (or only slightly lower than) [O₃]_{aft} (Caputi et al., 2019; He et al., 2022), while the average O₃ concentration in the NBL ([O₃]_{NBL}) should be much lower than [O₃]_{aft} due to the impacts of NO titration ($\Delta[O_3]_{titr}$) and dry deposition ($\Delta[O_3]_{dep}$), and the average O_x concentration in the NBL ([O_x]_{NBL}) should also be lower than [O₃]_{aft} due to dry deposition. The following relationships should be tenable:

$$[O_3]_{RL} \leq [O_3]_{aft} \quad (S1)$$

$$[O_3]_{NBL} = [O_3]_{aft} - \Delta[O_3]_{titr} - \Delta[O_3]_{dep} \quad (S2)$$

$$[O_x]_{NBL} = [O_3]_{aft} - \Delta[O_3]_{dep} \quad (S3)$$

Under disturbed condition with NOE but no STT impact (II), a downward transport of O₃ from the RL to NBL should be considered. Assuming that the downward transport causes a reduction of [O₃]_{RL} by $\Delta[O_3]_{D1}$ and an increase of [O₃]_{NBL} by $\Delta[O_3]_{D2}$, then

$$[O_3]_{RL} \leq [O_3]_{aft} - \Delta[O_3]_{D1} \quad (S4)$$

$$[O_3]_{NBL} = [O_3]_{aft} - \Delta[O_3]_{titr} - \Delta[O_3]_{dep} + \Delta[O_3]_{D2} \quad (S5)$$

$$[O_x]_{NBL} = [O_3]_{aft} - \Delta[O_3]_{dep} + \Delta[O_3]_{D2} \quad (S6)$$

Under disturbed condition with NOE and STT impact (III), net contributions of O₃ from the STT should be considered to the RL and the NBL. Assuming that the STT contribution increases [O₃]_{RL} and [O₃]_{NBL} by $\Delta[O_3]_{STT1}$ and $\Delta[O_3]_{STT2}$,

respectively, then

$$[O_3]_{RL} \leq [O_3]_{aft} + \Delta[O_3]_{STT1} \quad (S7)$$

$$[O_3]_{NBL} = [O_3]_{aft} - \Delta[O_3]_{titr} - \Delta[O_3]_{dep} \pm \Delta[O_3]_{STT2} \quad (S8)$$

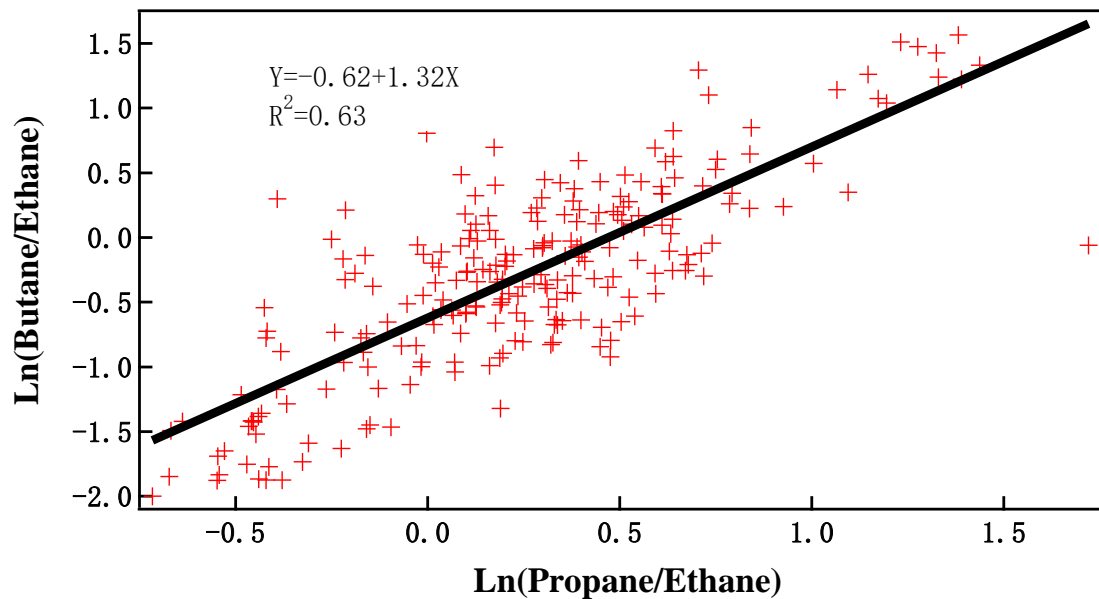
$$[O_x]_{NBL} = [O_3]_{aft} - \Delta[O_3]_{dep} + \Delta[O_3]_{STT2} \quad (S9)$$

Equation (S3) indicates that $[O_x]_{NBL}$ should be significantly lower than $[O_3]_{aft}$ under undisturbed conditions. Although equation (S6) shows that $[O_x]_{NBL}$ could be higher than $[O_3]_{aft}$ (i.e., if $\Delta[O_3]_{dep} < \Delta[O_3]_{D2}$), it cannot really occur because $[O_3]_{RL} < [O_3]_{aft}$ (see equation (S4)) and O_3 cannot be transported from a lower concentration position to the higher one. Therefore, $[O_x]_{NBL}$ should not be significantly higher than $[O_3]_{aft}$ under disturbed conditions with NOE but no STT impact. Dry deposition is only a small sink for nighttime surface O_3 in northern China (Tang et al., 2017), while a STT impact could substantially enhanced the level of surface O_3 if it reaches the surface layer. Hence, it is very likely according to equation (S9) that $[O_x]_{NBL}$ is significantly higher than $[O_3]_{aft}$ under disturbed condition with a STT impact. In summary, $[O_x]_{NBL}$ should be significantly higher than $[O_3]_{aft}$ if the NBL is really impacted by stratospheric O_3 , otherwise the STT impact is negligible even though a NOE event is observed.

Text S4S2. Estimating photochemical ages of air masses arrived at the Zibo supersite

Once emitted into the atmosphere, all hydrocarbons experience decay caused mainly by the oxidation of OH radical and atmospheric mixing (McKeen et al., 1990; Parrish et al., 1992). The relative compositions of hydrocarbons were used to study the histories of air masses over rural areas (Roberts et al., 1984) and remote marine areas (Rudolph et al., 1990). The so-called photochemical ages of air masses can be derived from observed ratios of hydrocarbons and OH mixing ratios either measured or estimated. However, the calculated photochemical ages may be significantly impacted by atmospheric mixing on the ratios during transport (McKeen and Liu, 1993). Nevertheless, the estimation of photochemical age based on hydrocarbon ratios in air masses has been a current practice in atmospheric researches (e.g., Kleinman et al., 2003; Irei et al., 2016). Here, we follow the practice to estimate photochemical ages of air masses arrived at the Zibo (ZB) supersite during the NOE reported in Chen et al. (2022) and a few days before and after.

Hourly measurements of hydrocarbons at the supersite between 25 July and 5 August 2021 were used to calculated hydrocarbon ratios. Good correlations were found among some of the hydrocarbon ratios. Among the alkanes ratios, the best correlation existed between $\ln(\text{Butane}/\text{Ethane})$ and $\ln(\text{Propane}/\text{Ethane})$, with $R^2=0.63$ (Figure S2S10). Among the aromatics ratios, the best correlation existed between $\ln(\text{o-Xylene}/\text{Benzene})$ and $\ln(\text{Ethylbenzene}/\text{Benzene})$, with $R^2=0.89$ (Figure S3S11). In addition, there were also excellent correlations between $\ln(\text{Butane})$ and $\ln(\text{Propane})$ ($R^2=0.78$, Figure S4S12) and between $\ln(\text{o-Xylene})$ and $\ln(\text{Ethylbenzene})$ ($R^2=0.85$, Figure S5S13). These results indicate that ethane, propane and n-butane observed the supersite were very likely from the same sources and so were benzene, ethylbenzene and o-Xylene. Therefore, it is proper to estimate photochemical ages using the ratios between these alkanes and aromatics. We derived photochemical ages from the ratios $[\text{Butane}]/[\text{Propane}]$ and $[\text{o-Xylene}]/[\text{Ethylbenzene}]$.



145 | Figure S2S10: Correlation between $\text{Ln}(\text{Butane/Ethane})$ and $\text{Ln}(\text{Propane/Ethane})$.

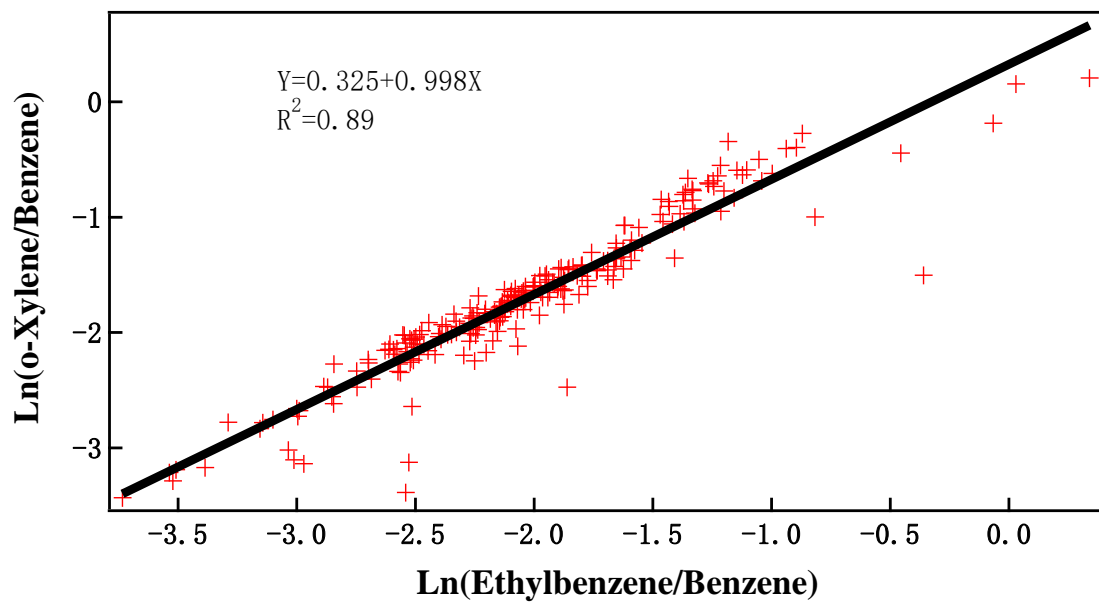


Figure S3S11: Correlation between $\text{Ln}(\text{o-Xylene/Benzene})$ and $\text{Ln}(\text{Ethylbenzene/Benzene})$.

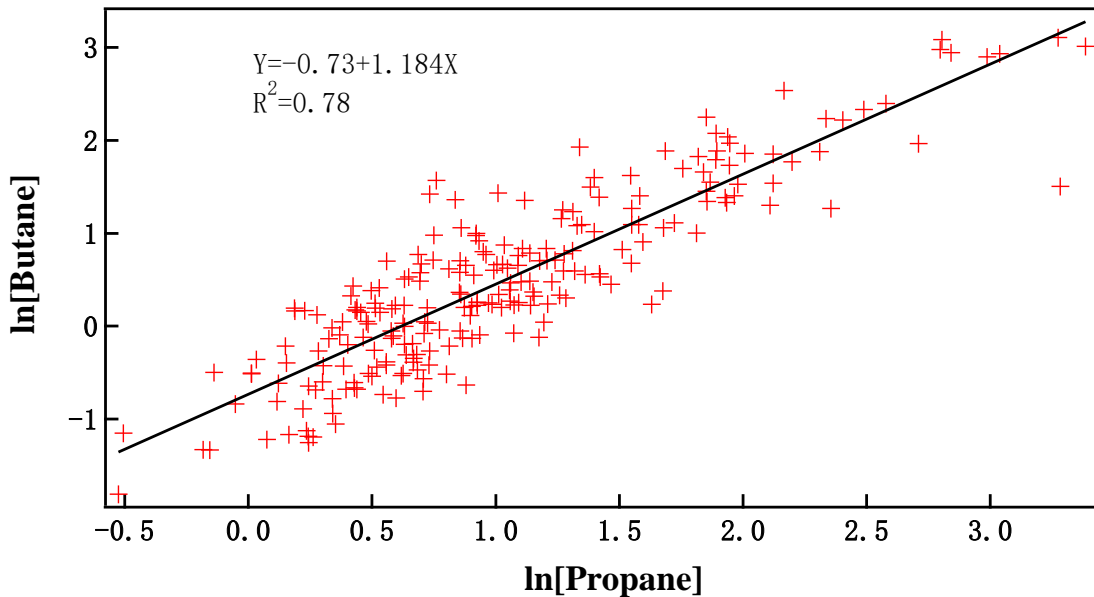


Figure S4S12: Correlation between butane and propane concentrations.

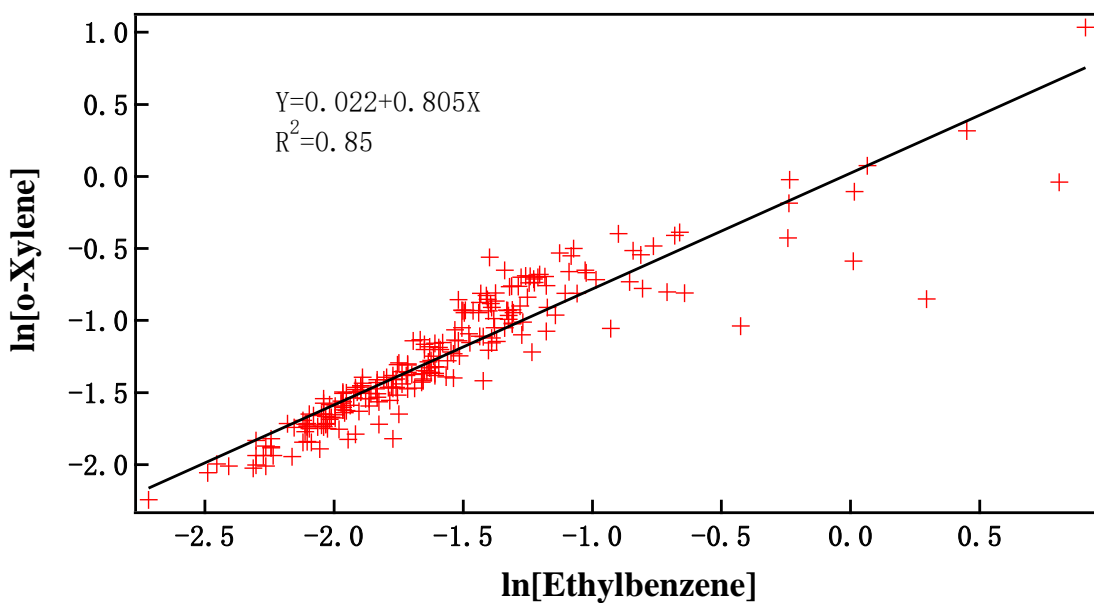


Figure S5S13: Correlation between o-xylene and ethylbenzene concentrations.

Since the concentration of hydrocarbon X is enhanced by emissions and lowered by reaction with OH and mixing with background air, the change of the X concentration with time can be generally expressed as:

$$\frac{d[X]}{dt} = S_x - k_x[\text{OH}][X], \quad (\text{S10})$$

where, $[X]$ is the concentration of X ; S_x represents collective impact on $[X]$ of physical processes such as emissions, dilution, etc.; $[\text{OH}]$ indicates the OH concentration averaged over the transport way; k_x is the rate constant for the $X+\text{OH}$ reaction. Similar expression can be given for hydrocarbon Y :

$$\frac{d[Y]}{dt} = S_y - k_y[\text{OH}][Y]$$

(S2S11)

In Eq. S10 and Eq. S2S11, S_x and S_y are unknown and difficult to obtain. However, their impacts on hydrocarbon concentrations are assumed to be low if the hydrocarbons are relatively reactive. After ignoring S_x and S_y in Eq. S10 and Eq. S2S11, the following equations can be obtained by integration from time 0 to t :

$$\ln [X] = \ln[X_0] - k_x[\text{OH}]t$$

(S3S12)

and

$$\ln [Y] = \ln[Y_0] - k_y[\text{OH}]t$$

(S4S13)

with X_0 and Y_0 being the respective concentrations of X and Y initial after emissions.

Finally, a formula for calculating photochemical ages can be derived from Eq. S3S12 and Eq. S4S13:

$$t = \frac{1}{(k_y - k_x)[\text{OH}]} \cdot \left(\ln \frac{[Y_0]}{[X_0]} - \ln \frac{[Y]}{[X]} \right)$$

(S5S14)

Rate constants (k_x and k_y) are available in literature. Table S1. lists the rate constants at 298K for the reactions of OH with n-butane, propane, ethylbenzene and o-xylene. These rate constants were used in the estimation of photochemical ages without considering the influences of atmospheric conditions.

Table S1: Rate constants of the reactions of the OH radical with some hydrocarbons at 298K

Reaction	Rate constant, $\text{cm}^3/\text{mol/s}$	Reference
n-butane + OH	1.45×10^{12}	Talukdar et al. (1994)
Propane + OH	6.58×10^{11}	DeMore et al. (1997)
ethylbenzene + OH	4.52×10^{12}	Atkinson (1986)
o-xylene + OH	8.85×10^{12}	Atkinson (1986)

180

There was no observation of OH radical over ZB and surroundings. An assumption had to be made for the value of $[\text{OH}]$ in Eq. S5S14. A recent study shows that the diel-average tropospheric column mean OH concentrations over the Yellow Sea and East China Sea areas were in the range of $(1.5-3) \times 10^6$ molecules/ cm^3 during July-August 2016 (Thompson et al., 2022). In-situ observations of vertical profiles of OH showed that the OH mixing ratio for 29 April 1994 varied roughly in the range

185 of $0.2\text{--}0.4$ pptv (about $(5\text{--}10)\times 10^6$ molecules/cm 3) at the altitudes from 1 km to 12 km over Oklahoma, USA, with no consistent gradients (Brune et al., 1998). Ground measurements in summer of 2014 at Wangdu, a rural site in the North China Plain, showed median values of OH varying from 5×10^5 molecules/cm 3 at night to 6.8×10^6 molecules/cm 3 during 12:00–16:00 LT (Tan et al., 2017). Earlier observations made in August 2006 at Yufa, a suburban site in Beijing, showed the OH level varying from 6×10^5 molecules/cm 3 (detection limit) at night to $(4\text{--}17)\times 10^6$ molecules/cm 3 around noontime (Lu et 190 al., 2013). Given these data of OH values, we assumed the average value of OH over ZB and surroundings for the period in consideration (i.e., 25 July – 5 August 2021) to be 5×10^6 molecules/cm 3 .

To obtain a better estimate of the range of photochemical ages, we calculated photochemical ages using both [Butane]/[Propane] and [o-Xylene]/[Ethylbenzene]. The initial values of [Butane]/[Propane] and [o-Xylene]/[Ethylbenzene] were not available. Therefore, we substituted the maximum [Butane]/[Propane] (2.25) and [o-Xylene]/[Ethylbenzene] (2.31) 195 for the initial values of [Butane]/[Propane] and [o-Xylene]/[Ethylbenzene], respectively. These maximum ratios should be lower than the initial ones because they represented ratios certain time after the hydrocarbons were emitted. This may more or less underestimate photochemical ages but does not change our conclusion.

The photochemical ages of air masses arrived at the ZB supersite during 25 July – 5 August 2021 were calculated using 200 Eq. [S5S14](#), and based on [Butane]/[Propane] and [o-Xylene]/[Ethylbenzene], respectively. The two sets of estimated photochemical ages are shown in Figure 3, together with the observed O₃ data.

References

205 Atkinson, R.: Kinetics and mechanisms of the gas-phase reactions of the hydroxyl radical with organic compounds under atmospheric conditions, *Chem. Rev.*, 86, 69, 1986.

Brune, W.H., Faloona, I.C., Tan, D., Weinheimer, A.J., Campos, T., Ridley, B.A., Vay, S.A., Collins, J.E., Sachse, G.W., 210 Jaegle, L., and Jacob, D.J.: Airborne in-situ OH and HO₂ observations in the cloud-free troposphere and lower stratosphere during SUCCESS, *Geophys. Res. Lett.*, 25(10), 1701–1704, 1998.

Caputi, D.J., Faloona, I., Trousdale, J., Smoot, J., Falk, N., and Conley, S.: Residual layer ozone, mixing, and the nocturnal jet in California's San Joaquin Valley, *Atmos. Chem. Phys.*, 19, 4721–4740, <https://doi.org/10.5194/acp-19-4721-2019>, 2019.

Chen, Z., Liu, J., Qie, X., Cheng, X., Shen, Y., Yang, M., Jiang, R., and Liu, X.: Transport of substantial stratospheric ozone to the surface by a dying typhoon and shallow convection, *Atmos. Chem. Phys.*, 22, 8221–8240, 215 <https://doi.org/10.5194/acp-22-8221-2022>, 2022.

DeMore, W.B., Sander, S.P., Golden, D.M., Hampson, R.F., Kurylo, M.J., Howard, C.J., Ravishankara, A.R., Kolb, C.E., and Molina, M.J.: Chemical kinetics and photochemical data for use in stratospheric modeling. Evaluation number 12, JPL Publication, 97-4 , 1-266, 1997.

220 He, C., Lu, X., Wang, H., Wang, H., Li, Y., He, G., He, Y., Wang, Y., Zhang, Y., Liu, Y., Fan, Q., and Fan, S.: The unexpected high frequency of nocturnal surface ozone enhancement events over China: characteristics and mechanisms, *Atmos. Chem. Phys.*, 22, 15243–15261, <https://doi.org/10.5194/acp-22-15243-2022>, 2022.

Irei, S., Takami, A., Sadanaga, Y., Nozoe, S., Yonemura, S., Bandow, H., and Yokouchi, Y.: Photochemical age of air pollutants, ozone, and secondary organic aerosol in transboundary air observed on Fukue Island, Nagasaki, Japan, *Atmos. Chem. Phys.*, 16, 4555–4568, <https://doi.org/10.5194/acp-16-4555-2016>, 2016.

225 Kleinman, L.I., Daum, P.H., Lee, Y.-N., Nunnermacher, L.J., Springston, S.R., Weinstein-Lloyd, J., Hyde, P., Doskey, P., Rudolph, J., Fst, J., and Berkowitz, C.: Photochemical age determinations in the Phoenix metropolitan area, *J. Geophys. Res.*, 108(D3), 4096, doi:10.1029/2002JD002621, 2003.

230 Lu, K. D., Hofzumahaus, A., Holland, F., Bohn, B., Brauers, T., Fuchs, H., Hu, M., Hässeler, R., Kita, K., Kondo, Y., Li, X., Lou, S. R., Oebel, A., Shao, M., Zeng, L. M., Wahner, A., Zhu, T., Zhang, Y. H., and Rohrer, F.: Missing OH source in a suburban environment near Beijing: observed and modelled OH and HO₂ concentrations in summer 2006, *Atmos. Chem. Phys.*, 13, 1057–1080, <https://doi.org/10.5194/acp-13-1057-2013>, 2013.

McKeen, S.A., and Liu, S.C.: Hydrocarbon ratios and photochemical history of air masses, *Geophys. Res. Lett.*, 20, 2363–2366, 1993.

235 McKeen, S.A., Trainer, M., E.Y. Hsie, R.K. Tallamraju, and S.C. Liu, On the indirect determination of atmospheric OH radical concentrations from reactive hydrocarbon measurements, *J. Geophys. Res.*, 95, 7493–7500, 1990.

Parrish, D.D., Hahn, C.J., Williams, E.J., Norton, R.B., Fehsenfeld, F.C., Singh, H.B., Shetter, J.D., Gandrun, B.W., and Ridley, B.A.: Indications of photochemical histories of pacific air masses from ~~measurements~~measurements of atmospheric trace species at Point Arena, California, *J. Geophys. Res.*, 97, 15883–15902, 1992.

240 Rolph, G., Stein, A., and Stunder, B.: Real-time Environmental Applications and Display sYstem: READY. *Environmental Modelling & Software*, 95, 210–228, <https://doi.org/10.1016/j.envsoft.2017.06.025>, 2017.

Roberts, J.M., Fehsenfeld, F.C., Liu, S.C., Bollinger, M.J., Hahn, C., Albritton, D.L., and Sievers, R.E.: Measurements of aromatic hydrocarbon ratios and NO_x concentrations in the rural troposphere: Observation of air mass photochemical aging and NO_x removal, *Atmos. Environ.*, 18, 2421–2432, 1984.

Rudolph, J., and Johnen, FJ: Measurements of light atmospheric hydrocarbons over the Atlantic in regions of low biological activity, *J. Geophys. Res.*, 95, 20583–20591, 1990.

245 Stein, A.F., Draxler, R.R., Rolph, G.D., Stunder, B.J.B., Cohen, M.D., and Ngan, F.: NOAA's HYSPLIT atmospheric transport and dispersion modeling system, *Bull. Amer. Meteor. Soc.*, 96, 2059–2077, <http://dx.doi.org/10.1175/BAMS-D-14-00110.1>, 2015.

250 Talukdar, R.K., Melouki, A., Gierczak, T., Barone, S., Chiang, S-Y., and Ravishankara, A.R.: Kinetics of the reactions of OH with alkanes, *Int. J. Chem. Kinet.*, 26, 973-990, 1994.

Tan, Z., Fuchs, H., Lu, K., Hofzumahaus, A., Bohn, B., Broch, S., Dong, H., Gomm, S., Häseler, R., He, L., Holland, F., Li, X., Liu, Y., Lu, S., Rohrer, F., Shao, M., Wang, B., Wang, M., Wu, Y., Zeng, L., Zhang, Y., Wahner, A., and Zhang, Y.: Radical chemistry at a rural site (Wangdu) in the North China Plain: observation and model calculations of OH, HO₂ and RO₂ radicals, *Atmos. Chem. Phys.*, 17, 663–690, <https://doi.org/10.5194/acp-17-663-2017>, 2017.

255 Thompson, C.R., Wofsy, S.C., Prather, M.J., Newman, P.A., Hanisco, T.F., Ryerson, T.B., Fahey, D.W., Apel, E.C., Brock, C.A., Brune, W.H., Froyd, K., Katich, J.M., Nicely, J.M., Peischl, J., Ray, E., Veres, P.R., Wang, S., Allen, H.M., Asher, E., Bian, H., Blake, D., Bourgeois, I., Budney, J., Bui, T.P., Butler, A., Campuzano-Jost, P., Chang, C., Chin, M., Commane, R., Correa, G., Crounse, J.D., Daube, B., Dibb, J.E., DiGangi, J.P., Diskin, G.S., Dollner, M., Elkins, J.W., Fiore, A.M., Flynn, C.M., Guo, H., Hall, S.R., Hannun, R.A., Hills, A., Hints, E.C., Hodzic, A., Hornbrook, R.S., Huey, L.G., Jimenez, J.L., Keeling, R.F., Kim, M.J., Kupc, A., Lace, F., Lait, L.R., Lamarque, J.-F., Liu, J., McKain, K., Meinardi, S., Miller, D.O., Montzka, S.A., Moore, F.L., Morgan, E.J., Murphy, D.M., Murray, L.T., Nault, B.A., Neuman, J.N., Nguyen, L., Gonzalez, Y., Rollins, A., Rosenlof, K., Sargent, M., Schill, G., Schwarz, J.P., St. Clair, J.M., Steenrod, S.D., Stephens, B.B., Strahan, S.E., Strode, S.A., Sweeney, C., Thames, A.B., Ullmann, K., Wagner, N., Weber, R., Weinzierl, B., Wennberg, P.O., Williamson, C.J., Wolfe, G.M., and Zeng, L.: The NASA Atmospheric Tomography (ATom) Mission Imaging the Chemistry of the Global Atmosphere, *Bulletin of American Meteorological Society*, E761-790, <https://doi.org/10.1175/BAMS-D-20-0315.1>, 2022.

Wang, H., Lu, K., Chen, X., Zhu, Q., Wu, Z., Wu, Y., and Sun, K.: Fast particulate nitrate formation via N₂O₅ uptake aloft in winter in Beijing, *Atmos. Chem. Phys.*, 18, 10483–10495, <https://doi.org/10.5194/acp-18-10483-2018>, 2018.